

Large-scale Heteroscedastic Regression via Gaussian Process

Haitao Liu, Yew-Soon Ong, *Fellow, IEEE*, and Jianfei Cai, *Senior Member, IEEE*

Abstract—Heteroscedastic regression which considers varying noises across input domain has many applications in fields like machine learning and statistics. Here we focus on the heteroscedastic Gaussian process (HGP) regression which integrates the latent function and the noise together in a unified non-parametric Bayesian framework. Though showing remarkable performance, HGP suffers from the cubic time complexity, which strictly limits its application to big data. To improve the scalability of HGP, we first develop a variational sparse inference algorithm, named VSHGP, to handle large-scale datasets. Furthermore, two variants are developed to further improve the scalability and capability of VSHGP. The first is stochastic VSHGP (SVSHGP) which derives a relaxed evidence lower bound factorized over data points, thus enhancing efficient stochastic variational inference. The second is distributed VSHGP (DVSHGP) which (i) follows the Bayesian committee machine formalism to distribute computations over multiple local VSHGP experts with many inducing points; and (ii) adopts hybrid parameters for experts to guard against over-fitting and capture local variety. Superiority of DVSHGP and SVSHGP as compared to existing scalable heteroscedastic/homoscedastic GPs is then verified using a synthetic dataset and four real-world datasets.

Index Terms—Heteroscedastic GP, Large-scale, Sparse approximation, Stochastic variational inference, Distributed learning.

I. INTRODUCTION

IN supervised learning, we learn a machine learning model from n training points $\mathbf{X} = \{\mathbf{x}_i\}_{i=1}^n$ defined in R^d and the observations $\mathbf{y} = \{y(\mathbf{x}_i) = f(\mathbf{x}_i) + \epsilon_i\}_{i=1}^n$, where f is the underlying function and ϵ_i is the independent noise. As a non-parametric Bayesian model, Gaussian process (GP) places a GP prior on f with $\epsilon_i \sim \mathcal{N}(0, \sigma_\epsilon^2)$, resulting in the standard, *homoscedastic* GP. The homoscedasticity offers tractable inference to enable extensive applications in regression and classification [1], visualization [2], Bayesian optimization [3], multi-task learning [4], active learning [5], etc.

Many realistic problems, e.g., volatility forecasting [6], biophysical variables estimation [7], cosmological redshifts estimation [8], robotics and vehicle control [9], [10], however often need to consider *input-dependent* noise rather than the highly restrictive *constant* noise.

To account for the heteroscedastic noise in GP, there exists two main strategies: (i) treat the GP as a black-box and interpret the heteroscedasticity using another separate model; and (ii) integrate the heteroscedasticity within the unifying GP

framework. The first post-model strategy first trains a standard GP to capture the underlying function f , and then either trains another GP to take the remaining empirical variance into account [11] or use the quantile regression [12] to model the lower and upper quantiles of the variance respectively.

In contrast, the second integration strategy provides an elegant framework for heteroscedastic regression. The simplest way to mimic variable noise is through adding independent yet different noise variances to the diagonal of kernel matrix, and learns a point estimation of them in the GP framework [13]. Goldberg et al. [14] introduced a more principled heteroscedastic GP (HGP) which infers a mean-field GP for $f(\mathbf{x})$ and an additional GP $g(\mathbf{x})$ for $\log \sigma_\epsilon^2(\mathbf{x})$ jointly. Note that unlike the homoscedastic GP, the inference in HGP is challenging since the model evidence (marginal likelihood) $p(\mathbf{y})$ and the posterior are intractable. To this end, various approximate inference methods, e.g., markov chain monte carlo (MCMC) [14], maximum a posteriori (MAP) [15]–[17], variational inference [18], [19], expectation propagation [20], [21] and Laplace approximation [22], have been used. The most accurate MCMC is quite slow when handling large-scale datasets; the MAP is a point estimation which does not integrate the latent variables out, leading to over-fitting and oscillation; the variational inference and its variants, which run fast via maximizing over a tractable and rigorous lower bound of the evidence, provide a trade-off. Apart from the HGP in [14], other HGPs which describe the heteroscedastic noise together with the non-stationary features using point-wise division of two latent functions have been proposed for example in [23], [24].

When handling n training points, the standard GP suffers from a cubic complexity $\mathcal{O}(n^3)$ due to the inversion of an $n \times n$ kernel matrix, which makes it unaffordable for big data. Since HGP employs an additional log-GP for noise variance, its complexity is about two times that of standard GP. Hence, to handle large-scale datasets, which is of great demand in the era of big data, the scalability of HGP should be improved.

Recently, there has been an increasing trend on the development of scalable GPs, which are classified into two core categories: global approximation and local approximation [25]. As the representative of global approximation, sparse approximation considers m ($m \ll n$) *global* inducing pairs $\{\mathbf{X}_m, \mathbf{f}_m\}$ to optimally summarize the training data by approximating the prior [26] or the posterior [27], resulting in the complexity of $\mathcal{O}(nm^2)$. Variants of sparse approximation have been recently proposed to handle millions of data points via distributed inference [28], [29], stochastic variational inference [30]–[32], or structured inducing points [33]. Due to the small set of

Haitao Liu is with the Rolls-Royce@NTU Corporate Lab, Nanyang Technological University, Singapore, 637460. E-mail: htliu@ntu.edu.sg

Yew-Soon Ong and Jianfei Cai are with School of Computer Science and Engineering, Nanyang Technological University, Singapore, 639798. E-mail: asysong@ntu.edu.sg; asjfc@ntu.edu.sg.

Manuscript received xxx, 2018; revised xxx, 2019.

global inducing points, sparse approximation, however, often faces challenges in capturing quick-varying features [34], [35]. On the other hand, local approximation, which is inspired by the idea of divide-and-conquer, first trains GP experts on local subsets and then collects and aggregates their predictions, for example by the means of product-of-experts (PoE) [36], Bayesian committee machine (BCM) [37]–[39] and mixture-of-experts (MoE) [40], [41]. Hence, local approximation not only distributes the computations but also captures quick-varying features well. Hybrid strategies thereafter have been presented for taking advantages of both global and local approximations [42]–[44].

The developments in scalable homoscedastic GPs have thus motivated us to scale up HGPs. Alternatively, we could combine the simple Subset-of-Data (SoD) approximation [45] with the empirical HGP [11] which trains two separate GPs for predicting mean and variance, respectively. The empirical variance however is hard to fit since it follows an asymmetric Gaussian distribution. More reasonably, the GP using variable covariances (GPVC) [8] follows the idea of relevance vector machine (RVM) [46] that a stationary kernel $k(\cdot, \cdot)$ has a positive and finite Fourier spectrum, suggesting using only m_b ($m_b \ll n$) independent basis functions for approximating both f and g . Note that GPVC shares the basis functions for f and g which however might produce distinct features. Besides, the RVM-type model usually suffers from underestimated prediction variance when leaving \mathbf{X} [47].

Apart from the above scalable HGPs, there are some scalable “pseudo” HGPs [42], [48] which are not designed for such case, but can describe the heteroscedastic noise to some extent due to the factorized conditionals. For instance, the Fully Independent Training Conditional (FITC) [48] adopts a factorized training conditional $p(\mathbf{f}|\mathbf{f}_m) \approx \prod_{i=1}^n p(f_i|\mathbf{f}_m)$,¹ resulting in a varying noise term [49]. Though equipped with heteroscedastic variance,² the FITC (i) severely underestimates the constant noise variance, and (ii) sacrifices the prediction mean [49]. Furthermore, the block version of FITC, named Partially Independent Conditional (PIC) [42], partitions the data $\mathcal{D} = \{\mathbf{X}, \mathbf{y}\}$ into M subsets (blocks) $\{\mathcal{D}_i\}_{i=1}^M$, and then adopts a new factorized conditional $p(\mathbf{f}, \mathbf{f}_*|\mathbf{f}_m) \approx p(\mathbf{f}_{\mathcal{D}_j}, \mathbf{f}_*|\mathbf{f}_m) \prod_{i=1}^M p(\mathbf{f}_{\mathcal{D}_i}|\mathbf{f}_m)$ when the test point \mathbf{x}_* falls into the subregion defined by \mathcal{D}_j , resulting in a hybrid of local and global approximations. The block-dependent PIC however may produce discontinuous predictions on block boundaries [43]. Recently, the stochastic/distributed variants of FI(T)C and PIC have been developed to further improve the scalability [29], [31], [44], [50].

This paper presents scalable variational sparse HGPs for large-scale regression. Particularly, we make the following contributions:

1. A variational and sparse inference algorithm for HGP, named VSHGP, is developed. Specifically, VSHGP derives an analytical evidence lower bound (ELBO) using m inducing

points for f and u inducing points for g , resulting in a greatly reduced complexity of $\mathcal{O}(nm^2 + nu^2)$. Besides, some tricks for example re-parameterization are used to ease the inference;

2. A stochastic variant SVSHGP is further proposed to improve the scalability of VSHGP. Specifically, we keep a relaxed ELBO, which factorizes over data points, thus enhancing efficient stochastic variational inference;

3. A distributed variant DVSHGP is also proposed for improving both the scalability and the capability of VSHGP. The local experts with many inducing points (i) distribute computations for parallel computing, and (ii) employ hybrid parameters to guard against over-fitting and capture local variety;

4. Extensive experiments conducted on datasets with up to two million points reveal that the localized DVSHGP exhibits superior performance, while the global SVSHGP may sacrifice the prediction mean for capturing heteroscedastic noise.

5. Implementations of DVSHGP and SVSHGP are provided at <https://github.com/LiuHaiTao01>.³

The remainder of the article is organized as follows. Section II first introduces a variational sparse inference framework for HGP, named VSHGP. Then, we develop the stochastic variant in Section III and the distributed variant in Section IV for further enhancing the scalability and capability. Thereafter, Section VI verifies the their performance on a synthetic dataset, three medium real-world datasets and a large-scale dataset. Finally, Section VII provides concluding remarks.

II. VARIATIONAL SPARSE HGP

A. Sparse approximation

We follow [14] to define an HGP $y(\mathbf{x}) = f(\mathbf{x}) + \epsilon(\mathbf{x})$, wherein the latent function $f(\mathbf{x})$ and the noise $\epsilon(\mathbf{x})$ follow

$$f(\mathbf{x}) \sim \mathcal{GP}(0, k_f(\mathbf{x}, \mathbf{x}')), \quad \epsilon(\mathbf{x}) \sim \mathcal{N}(0, \sigma_\epsilon^2(\mathbf{x})). \quad (1)$$

It is observed that the input-dependent noise variance $\sigma_\epsilon^2(\mathbf{x})$ enables describing heteroscedasticity. Notably, the HGP in (1) degenerates to homoscedastic GP when we restrict $\sigma_\epsilon^2(\mathbf{x})$ to be constant for any \mathbf{x} . To ensure the positivity of noise variance, we particularly consider the exponential form $\sigma_\epsilon^2(\mathbf{x}) = e^{g(\mathbf{x})}$, wherein the latent function $g(\mathbf{x})$ akin to $f(\mathbf{x})$ follows an independent GP prior

$$g(\mathbf{x}) \sim \mathcal{GP}(\mu_0, k_g(\mathbf{x}, \mathbf{x}')). \quad (2)$$

The only difference is that unlike the zero-mean GP prior placed on $f(\mathbf{x})$, we explicitly consider a prior mean μ_0 to account for the variability of the noise variance.⁴ The kernels k_f and k_g could be, e.g., the squared exponential (SE) function equipped with automatic relevance determination (ARD)

$$k(\mathbf{x}, \mathbf{x}') = \sigma_s^2 \exp\left(-\frac{1}{2} \sum_{i=1}^d \frac{(x_i - x'_i)^2}{l_i^2}\right), \quad (3)$$

¹The Fully Independent Conditional (FIC) [26] additionally applies the factorization to test conditional as $p(\mathbf{f}_*|\mathbf{f}_m) \approx \prod_{i=1}^{n_*} p(f_{i*}|\mathbf{f}_m)$ where n_* is the number of test points.

²We do not say “heteroscedastic noise variance” since FITC still employs a constant noise $\epsilon_i \sim \mathcal{N}(0, \sigma_\epsilon^2)$ for $1 \leq i \leq n$.

³The SVSHGP is implemented based on GFlow [51], which benefits from parallel/GPU speedup and automatic differentiation of Tensorflow [52]. The DVSHGP is built upon the GPML toolbox [53].

⁴For f , we can pre-process the data to fulfill the zero-mean assumption. For g , however, it is hard to satisfy the zero-mean assumption, since we have no access to the “noise” data.

where the signal variance σ_s^2 is an output scale, and the length-scale l_i is an input scale along the i th dimension.

Given the training data $\mathcal{D} = \{\mathbf{X}, \mathbf{y}\}$, the joint priors follow

$$p(\mathbf{f}) = \mathcal{N}(\mathbf{f}|\mathbf{0}, \mathbf{K}_{nn}^f), \quad p(\mathbf{g}) = \mathcal{N}(\mathbf{g}|\mu_0\mathbf{1}, \mathbf{K}_{nn}^g), \quad (4)$$

where $[\mathbf{K}_{nn}^f]_{ij} = k_f(\mathbf{x}_i, \mathbf{x}_j)$ and $[\mathbf{K}_{nn}^g]_{ij} = k_g(\mathbf{x}_i, \mathbf{x}_j)$ for $1 \leq i, j \leq n$. Accordingly, the data likelihood becomes

$$p(\mathbf{y}|\mathbf{f}, \mathbf{g}) = \mathcal{N}(\mathbf{y}|\mathbf{f}, \Sigma_\epsilon), \quad (5)$$

where the diagonal noise matrix has $[\Sigma_\epsilon]_{ii} = \exp(g(\mathbf{x}_i))$.

To scale up HGP, we follow the sparse approximation framework to introduce m inducing variables $\mathbf{f}_m \sim \mathcal{N}(\mathbf{f}_m|\mathbf{0}, \mathbf{K}_{mm}^f)$ at the inducing points \mathbf{X}_m for \mathbf{f} ; similarly, we introduce u inducing variables $\mathbf{g}_u \sim \mathcal{N}(\mathbf{g}_u|\mu_0\mathbf{1}, \mathbf{K}_{uu}^g)$ at the independent \mathbf{X}_u for \mathbf{g} . Besides, we assume that \mathbf{f}_m is a sufficient statistic for \mathbf{f} , and \mathbf{g}_u a sufficient statistic for \mathbf{g} .⁵ As a result, we obtain two training conditionals

$$p(\mathbf{f}|\mathbf{f}_m) = \mathcal{N}(\mathbf{f}|\Omega_{nm}^f \mathbf{f}_m, \mathbf{K}_{nn}^f - \mathbf{Q}_{nn}^f), \quad (6a)$$

$$p(\mathbf{g}|\mathbf{g}_u) = \mathcal{N}(\mathbf{g}|\Omega_{nu}^g (\mathbf{g}_u - \mu_0\mathbf{1}) + \mu_0\mathbf{1}, \mathbf{K}_{nn}^g - \mathbf{Q}_{nn}^g), \quad (6b)$$

where $\Omega_{nm}^f = \mathbf{K}_{nm}^f (\mathbf{K}_{mm}^f)^{-1}$, $\Omega_{nu}^g = \mathbf{K}_{nm}^g (\mathbf{K}_{mm}^g)^{-1}$, $\mathbf{Q}_{nn}^f = \mathbf{K}_{nm}^f (\mathbf{K}_{mm}^f)^{-1} \mathbf{K}_{mn}^f$ and $\mathbf{Q}_{nn}^g = \mathbf{K}_{nm}^g (\mathbf{K}_{mm}^g)^{-1} \mathbf{K}_{mn}^g$.

In sparse HGP with augmented probability space, the model evidence

$$p(\mathbf{y}) = \int p(\mathbf{y}|\mathbf{f}, \mathbf{g}) p(\mathbf{f}|\mathbf{f}_m) p(\mathbf{g}|\mathbf{g}_u) p(\mathbf{f}_m) p(\mathbf{g}_u) d\mathbf{f}_m d\mathbf{g}_u,$$

together with the posterior $p(\mathbf{z}|\mathbf{y}) = p(\mathbf{y}|\mathbf{z})p(\mathbf{z})/p(\mathbf{y})$ where $\mathbf{z} = \{\mathbf{f}, \mathbf{g}, \mathbf{f}_m, \mathbf{g}_u\}$, however, is intractable. Hence, we next derive a variational sparse inference algorithm to obtain an analytical lower bound of $\log p(\mathbf{y})$.

B. Evidence lower bound

A central task in sparse HGP is the evaluation of the posterior $p(\mathbf{z}|\mathbf{y})$. Under the sufficient statistic assumption, we arrive at $p(\mathbf{z}|\mathbf{y}) = p(\mathbf{f}|\mathbf{f}_m)p(\mathbf{g}|\mathbf{g}_u)p(\mathbf{f}_m|\mathbf{y})p(\mathbf{g}_u|\mathbf{y})$. Due to the intractability of $p(\mathbf{z}|\mathbf{y})$ in practice, we employ the mean-field theory [54] to approximate $p(\mathbf{z}|\mathbf{y})$ as

$$q(\mathbf{z}) = p(\mathbf{f}|\mathbf{f}_m)p(\mathbf{g}|\mathbf{g}_u)q(\mathbf{f}_m)q(\mathbf{g}_u), \quad (7)$$

where $q(\mathbf{f}_m)$ and $q(\mathbf{g}_u)$ are free variational distributions to approximate the posteriors $p(\mathbf{f}_m|\mathbf{y})$ and $p(\mathbf{g}_u|\mathbf{y})$, respectively.

In order to push the approximation $q(\mathbf{z})$ towards the exact distribution $p(\mathbf{z}|\mathbf{y})$, we minimize their Kullback-Leibler (KL) divergence $\text{KL}(q(\mathbf{z})||p(\mathbf{z}|\mathbf{y}))$, which, on the other hand, is equivalent to maximizing the ELBO F , since $\text{KL}(\cdot, \cdot) \geq 0$, as

$$F = \int q(\mathbf{z}) \log \frac{p(\mathbf{z}, \mathbf{y})}{q(\mathbf{z})} d\mathbf{z} = \log p(\mathbf{y}) - \text{KL}(q(\mathbf{z})||p(\mathbf{z}|\mathbf{y})). \quad (8)$$

As a consequence, instead of directly maximizing the intractable $\log p(\mathbf{y})$ for inference, we now seek the maximization of F w.r.t. the variational distributions $q(\mathbf{f}_m)$ and $q(\mathbf{g}_u)$.

⁵Sufficient statistic means the variables \mathbf{z} and \mathbf{f} are independent given \mathbf{f}_m , i.e., it holds $p(\mathbf{z}|\mathbf{f}, \mathbf{f}_m) = p(\mathbf{z}|\mathbf{f}_m)$.

By reformulating F we observe that

$$F = -\text{KL}(q(\mathbf{f}_m)||q^*(\mathbf{f}_m)) + H(q(\mathbf{g}_u)) + \text{const.}, \quad (9)$$

where $H(q(\mathbf{g}_u))$ is the information entropy of $q(\mathbf{g}_u)$, and $q^*(\mathbf{f}_m)$ satisfies

$$q^*(\mathbf{f}_m) = \frac{p(\mathbf{f}_m)}{C_0} e^{\int p(\mathbf{f}|\mathbf{f}_m)p(\mathbf{g}|\mathbf{g}_u)q(\mathbf{g}_u) \log p(\mathbf{y}|\mathbf{f}, \mathbf{g}) d\mathbf{f} d\mathbf{g} d\mathbf{g}_u}, \quad (10)$$

where C_0 is a normalization constant to make $q^*(\mathbf{f}_m)$ be a valid probability density function (PDF). Observing (9), we find that given $q(\mathbf{g}_u)$, $q^*(\mathbf{f}_m)$ is the optimal distribution since it maximizes the bound F .

Therefore, by substituting $q^*(\mathbf{f}_m)$ back into F , we arrive at a tighter ELBO, given $q(\mathbf{g}_u) = \mathcal{N}(\mathbf{g}_u|\mu_u, \Sigma_u)$, as

$$\begin{aligned} F_V &= \log C_0 - \text{KL}(q(\mathbf{g}_u)||p(\mathbf{g}_u)) \\ &= \underbrace{\log \mathcal{N}(\mathbf{y}|\mathbf{0}, \mathbf{Q}_{nn}^f + \mathbf{R}_g)}_{\text{log term}} - \underbrace{0.25 \text{Tr}[\Sigma_g]}_{\text{trace term of } \mathbf{g}} \\ &\quad - \underbrace{0.5 \text{Tr}[\mathbf{R}_g^{-1}(\mathbf{K}_{nn}^f - \mathbf{Q}_{nn}^f)]}_{\text{trace term of } \mathbf{f}} - \underbrace{\text{KL}(q(\mathbf{g}_u)||p(\mathbf{g}_u))}_{\text{KL term}}, \end{aligned} \quad (11)$$

where \mathbf{R}_g is an $n \times n$ diagonal matrix with $[\mathbf{R}_g]_{ii} = e^{[\mu_g]_i - [\Sigma_g]_{ii}/2}$, and the mean and variance

$$\mu_g = \Omega_{nu}^g (\mu_u - \mu_0\mathbf{1}) + \mu_0\mathbf{1}, \quad (12a)$$

$$\Sigma_g = \mathbf{K}_{nn}^g - \mathbf{Q}_{nn}^g + \Omega_{nu}^g \Sigma_u (\Omega_{nu}^g)^\top, \quad (12b)$$

come from $q(\mathbf{g}) = \int p(\mathbf{g}|\mathbf{g}_u)q(\mathbf{g}_u)d\mathbf{g}_u$ which approximates $p(\mathbf{g}|\mathbf{y})$. It is observed that the analytical bound F_V depends only on $q(\mathbf{g}_u)$ since we have ‘‘marginalized’’ $q(\mathbf{f}_m)$ out.

Let us delve further into the terms of F_V in (11):

- The log term $\log \mathcal{N}(\mathbf{y}|\mathbf{0}, \Sigma_y)$, where $\Sigma_y = \mathbf{Q}_{nn}^f + \mathbf{R}_g$, is analogous to that in a standard GP. It achieves bias-variance trade-off for both \mathbf{f} and \mathbf{g} by penalizing model complexity and low data likelihood [1].
- The two trace terms act as a regularization, which helps choose good inducing sets for \mathbf{f} and \mathbf{g} , and guard against over-fitting. It is observed that $\text{Tr}[\mathbf{K}_{nn}^g - \mathbf{Q}_{nn}^g]$ and $\text{Tr}[\mathbf{K}_{nn}^f - \mathbf{Q}_{nn}^f]$ represent the total variance of the training conditionals $p(\mathbf{g}|\mathbf{g}_u)$ and $p(\mathbf{f}|\mathbf{f}_m)$, respectively. In order to maximize F_V , the trace terms should be very small, which implies that \mathbf{f}_m and \mathbf{g}_u must be very informative (i.e., sufficient statistics) for \mathbf{f} and \mathbf{g} , called variational compression [55]. Particularly, the zero traces indicate that $\mathbf{f}_m = \mathbf{f}$ and $\mathbf{g}_u = \mathbf{g}$, thus recovering the variational HGP (VHGP) in [18]. Besides, the zero trace terms imply that the variances of $q(\mathbf{g}_u)$ equal to that of $p(\mathbf{g}_u|\mathbf{y})$.
- The KL term is a constraint for rationalising $q(\mathbf{g}_u)$. It is observed that minimizing the trace terms only pushes the variances of $q(\mathbf{g}_u)$ towards that of $p(\mathbf{g}_u|\mathbf{y})$. To let the covariances of $q(\mathbf{g}_u)$ rationally approximate that of $p(\mathbf{g}_u|\mathbf{y})$, the minimization of the KL term penalizes $q(\mathbf{g}_u)$ so that it does not deviate significantly from the prior $p(\mathbf{g}_u)$.

C. Reparameterization and inference

In order to maximize the ELBO F_V in (11), we need to infer $w = u + u(u + 1)/2$ free variational parameters in μ_u

and Σ_u , i.e., the number of variational parameters is quadratic to the inducing size for g . Assume that $u = 0.01n$, then w is larger than n when the training size $n > 2 \times 10^4$, leading to a high-dimensional and non-trivial optimization task.

We observe that the derivatives of F_V w.r.t. μ_u and Σ_u are

$$\begin{aligned}\frac{\partial F_V}{\partial \mu_u} &= \frac{1}{2}(\Omega_{nu}^g)^\top \Lambda_{nn}^{ab} \mathbf{1} - (\mathbf{K}_{uu}^g)^{-1}(\mu_u - \mu_0 \mathbf{1}), \\ \frac{\partial F_V}{\partial \Sigma_u} &= -\frac{1}{4}(\Omega_{nu}^g)^\top (\Lambda_{nn}^{ab} + \mathbf{I}) \Omega_{nu}^g + \frac{1}{2}[\Sigma_u^{-1} - (\mathbf{K}_{uu}^g)^{-1}],\end{aligned}$$

where the diagonal matrix $\Lambda_{nn}^{ab} = \Lambda_{nn}^a + \Lambda_{nn}^b$ with $\Lambda_{nn}^a = (\Sigma_y^{-1} \mathbf{y} \mathbf{y}^\top \Sigma_y^{-1} - \Sigma_y^{-1}) \odot \mathbf{R}_g$, $\Lambda_{nn}^b = (\mathbf{K}_{nn}^f - \mathbf{Q}_{nn}^f) \odot \mathbf{R}_g^{-1}$, and the operator \odot represents element-wise product. Hence, it is observed that μ_u and Σ_u^{-1} satisfy

$$\mu_u = 0.5 \mathbf{K}_{un}^g \Lambda_{nn}^{ab} \mathbf{1} + \mu_0 \mathbf{1}, \quad (13a)$$

$$\Sigma_u^{-1} = 0.5 (\Omega_{nu}^g)^\top (\Lambda_{nn}^{ab} + \mathbf{I}) \Omega_{nu}^g + (\mathbf{K}_{uu}^g)^{-1}, \quad (13b)$$

at the maximum of F_V . Interestingly, we find that both the optimal μ_u and Σ_u depend on the diagonal matrix $\Lambda_{nn} = 0.5(\Lambda_{nn}^{ab} + \mathbf{I})$, which is a positive semi-definite diagonal matrix, see the *non-negativity* proof of Λ_{nn} in Appendix A. Hence, we re-parameterize μ_u and Σ_u in terms of Λ_{nn} as

$$\mu_u = \mathbf{K}_{un}^g (\Lambda_{nn} - 0.5 \mathbf{I}) \mathbf{1} + \mu_0 \mathbf{1}, \quad (14a)$$

$$\Sigma_u^{-1} = (\mathbf{K}_{uu}^g)^{-1} + (\Omega_{nu}^g)^\top \Lambda_{nn} \Omega_{nu}^g. \quad (14b)$$

The re-parameterization in (14a) and (14b) eases the model inference by (i) reducing the number of variational parameters from ω to n , and (ii) limiting the new variational parameters Λ_{nn} to be non-negative, thus narrowing the search space.

So far, the bound F_V depends on the variational parameters Λ_{nn} , the kernel parameters θ_f and θ_g , the mean parameter μ_0 for g , and the inducing points \mathbf{X}_m and \mathbf{X}_u . We maximize F_V to infer all these hyperparameters $\psi = \{\Lambda_{nn}, \theta_f, \theta_g, \mathbf{X}_m, \mathbf{X}_u\}$ jointly for model selection. This non-linear optimization task can be solved via conjugate gradient descent (CGD), since the derivatives of F_V w.r.t. these hyperparameters have closed forms, see Appendix B.

D. Predictive Distribution

The predictive distribution $p(y_* | \mathbf{y}, \mathbf{x}_*)$ at the test point \mathbf{x}_* is approximated as

$$q(y_*) = \int p(y_* | f_*, g_*) q(f_*) q(g_*) df_* dg_*. \quad (15)$$

As for $q(f_*) = \int p(f_* | \mathbf{f}_m) q^*(\mathbf{f}_m) d\mathbf{f}_m$, we first calculate $q^*(\mathbf{f}_m)$ from (10) as

$$\begin{aligned}q^*(\mathbf{f}_m) &\propto p(\mathbf{f}_m) \mathcal{N}(\mathbf{y} | \Omega_{nm}^f \mathbf{f}_m, \mathbf{R}_g) \\ &\propto e^{\{-\frac{1}{2} \mathbf{f}_m^\top [(\mathbf{K}_{mm}^f)^{-1} + (\Omega_{nm}^f)^\top \mathbf{R}_g^{-1} \Omega_{nm}^f] \mathbf{f}_m + \mathbf{f}_m^\top (\Omega_{nm}^f)^\top \mathbf{R}_g^{-1} \mathbf{y}\}}.\end{aligned}$$

Through the ‘‘completing the square’’ operation, we recognize this Gaussian distribution as

$$q^*(\mathbf{f}_m) = \mathcal{N}(\mathbf{f}_m | \mathbf{K}_{mm}^f \mathbf{K}_R^{-1} \mathbf{K}_{mn}^f \mathbf{R}_g^{-1} \mathbf{y}, \mathbf{K}_{mm}^f \mathbf{K}_R^{-1} \mathbf{K}_{mm}^f), \quad (16)$$

where $\mathbf{K}_R = \mathbf{K}_{mn}^f \mathbf{R}_g^{-1} \mathbf{K}_{nm}^f + \mathbf{K}_{mm}^f$. Using (16), we have $q(f_*) = \mathcal{N}(f_* | \mu_{f_*}, \sigma_{f_*}^2)$ with

$$\mu_{f_*} = \mathbf{k}_{*m}^f \mathbf{K}_R^{-1} \mathbf{K}_{mn}^f \mathbf{R}_g^{-1} \mathbf{y}, \quad (17a)$$

$$\sigma_{f_*}^2 = \mathbf{k}_{**}^f - \mathbf{k}_{*m}^f (\mathbf{K}_{mm}^f)^{-1} \mathbf{k}_{m*}^f + \mathbf{k}_{*m}^f \mathbf{K}_R^{-1} \mathbf{k}_{m*}^f. \quad (17b)$$

It is interesting to find in (17b) that the correction term $\mathbf{k}_{*m}^f \mathbf{K}_R^{-1} \mathbf{k}_{m*}^f$ contains the heteroscedasticity information from the noise term \mathbf{R}_g . Hence, $q(f_*)$ produces *heteroscedastic* variances over the input domain, see an illustration example in Fig. 2(b). The heteroscedastic $\sigma_{f_*}^2$ (i) eases the learning of g , and (ii) plays as an auxiliary role, since the heteroscedasticity is mainly explained by g .⁶ Also, VSHGP is believed to produce a better prediction mean μ_{f_*} through the interaction between f and g in (17a).⁷

Similarly, we have the predictive distribution $q(g_*) = \int p(g_* | \mathbf{g}_u) q(\mathbf{g}_u) d\mathbf{g}_u = \mathcal{N}(g_* | \mu_{g_*}, \sigma_{g_*}^2)$ where, given $\mathbf{K}_\Lambda = \mathbf{K}_{un}^g \Lambda_{nn}^{-1} \mathbf{K}_{nu}^g + \mathbf{K}_{uu}^g$,

$$\mu_{g_*} = \mathbf{k}_{*u}^g (\mathbf{K}_{uu}^g)^{-1} (\mu_u - \mu_0 \mathbf{1}) + \mu_0 \mathbf{1}, \quad (18a)$$

$$\sigma_{g_*}^2 = \mathbf{k}_{**}^g - \mathbf{k}_{*u}^g (\mathbf{K}_{uu}^g)^{-1} \mathbf{k}_{u*}^g + \mathbf{k}_{*u}^g \mathbf{K}_\Lambda^{-1} \mathbf{k}_{u*}^g. \quad (18b)$$

Finally, using the posteriors $q(f_*)$ and $q(g_*)$, and the likelihood $p(y_* | f_*, g_*) = \mathcal{N}(y_* | f_*, e^{g_*})$, we have

$$q(y_*) = \int \mathcal{N}(y_* | \mu_{f_*}, e^{g_*} + \sigma_{f_*}^2) \mathcal{N}(g_* | \mu_{g_*}, \sigma_{g_*}^2) dg_*, \quad (19)$$

which is intractable and *non-Gaussian*. However, the integral can be approximated up to several digits using Gauss-Hermite quadrature, resulting in the mean and variance as [18]

$$\mu(\mathbf{x}_*) = \mu_{f_*}, \quad (20a)$$

$$\sigma^2(\mathbf{x}_*) = \sigma_{f_*}^2 + e^{\mu_{g_*} + \sigma_{g_*}^2/2}. \quad (20b)$$

In the final prediction variance $\sigma^2(\mathbf{x}_*)$, $\sigma_{f_*}^2$ mainly represents the uncertainty about f due to data density, and theoretically it approaches zero with increasing n ; the exponential term brings about the intrinsic heteroscedastic noise uncertainty.

It is notable that the unifying VSHGP includes VHGP [18] and variational sparse GP (VSGP) [27] as special cases: when $\mathbf{f}_m = \mathbf{f}$ and $\mathbf{g}_u = \mathbf{g}$, VSHGP recovers VHGP; when $q(\mathbf{g}_u) = p(\mathbf{g}_u)$, i.e., we are now facing a homoscedastic regression task, VSHGP regenerates to VSGP.

Overall, by introducing inducing sets for both \mathbf{f} and \mathbf{g} , VSHGP is equipped with the means to handle large-scale heteroscedastic regression. However, (i) with current time complexity $\mathcal{O}(nm^2 + nu^2)$, which is linear with training size, VSHGP is still unaffordable for large-scale datasets with, e.g., millions of data points; and (ii) as a global approximation, the capability of VSHGP is limited by the *small* and *global* inducing set.

To this end, we will introduce below two strategies to further improve the scalability and capability of VSHGP.

⁶The formulation of $\sigma_{f_*}^2$ in (17b) is similar to that of FITC [49]. But differently, since FITC employs a constant noise variance, the heteroscedasticity can only be explained by $\sigma_{f_*}^2$.

⁷This happens when g is learned well, see the numerical experiments below.

III. STOCHASTIC VSHGP

To further improve the *scalability* of VSHGP, the variational distribution $q(\mathbf{f}_m) = \mathcal{N}(\mathbf{f}_m | \boldsymbol{\mu}_m, \boldsymbol{\Sigma}_m)$ is re-introduced to keep using the original bound $F = \int q(\mathbf{z}) \log \frac{p(\mathbf{z}, \mathbf{y})}{q(\mathbf{z})} d\mathbf{z}$ in (8). Given the factorizations $q(\mathbf{z}) = p(\mathbf{f} | \mathbf{f}_m) p(\mathbf{g} | \mathbf{g}_u) q(\mathbf{f}_m) q(\mathbf{g}_u)$ and $p(\mathbf{y} | \mathbf{f}, \mathbf{g}) = \prod_{i=1}^N p(y_i | f_i, g_i)$, the ELBO F herein is

$$F = \sum_{i=1}^n \left[\log \mathcal{N}(y_i | [\boldsymbol{\mu}_f]_i, [\mathbf{R}_g]_{ii}) - \frac{1}{4} [\boldsymbol{\Sigma}_g]_{ii} - \frac{1}{2} [\boldsymbol{\Sigma}_f \mathbf{R}_g^{-1}]_{ii} \right] - \text{KL}[q(\mathbf{f}_m) | p(\mathbf{f}_m)] - \text{KL}[q(\mathbf{g}_u) | p(\mathbf{g}_u)], \quad (21)$$

with $\boldsymbol{\mu}_f = \boldsymbol{\Omega}_{nm}^f \boldsymbol{\mu}_m$ and $\boldsymbol{\Sigma}_f = \mathbf{K}_{nn}^f - \mathbf{Q}_{nn}^f + \boldsymbol{\Omega}_{nm}^f \boldsymbol{\Sigma}_m (\boldsymbol{\Omega}_{nm}^f)^\top$.

The new F is a relaxed version of F_V in (11). It is found that the derivatives of F w.r.t $\boldsymbol{\mu}_m$ and $\boldsymbol{\Sigma}_m$ satisfy

$$\frac{\partial F}{\partial \boldsymbol{\mu}_m} = (\boldsymbol{\Omega}_{nm}^f)^\top \mathbf{R}_g^{-1} (\mathbf{y} - \boldsymbol{\Omega}_{nm}^f \boldsymbol{\mu}_m) - (\mathbf{K}_{mm}^f)^{-1} \boldsymbol{\mu}_m, \quad (22a)$$

$$\frac{\partial F}{\partial \boldsymbol{\Sigma}_m} = -\frac{1}{2} (\boldsymbol{\Omega}_{nm}^f)^\top \mathbf{R}_g^{-1} \boldsymbol{\Omega}_{nm}^f + \frac{1}{2} (\boldsymbol{\Sigma}_m^{-1} - (\mathbf{K}_{mm}^f)^{-1}). \quad (22b)$$

Let the gradients be zeros, we recover the optimal solution $q^*(\mathbf{f}_m)$ in (16), indicating that $F_V \geq F$ with the equality at $q(\mathbf{f}_m) = q^*(\mathbf{f}_m)$.

The scalability is improved by F through the first term in the right-hand side of (21), which factorizes over data points. The sum form allows using efficient stochastic gradient descent (SGD), e.g., Adam [56], with mini-batch mode for big data. Specifically, we choose a random subset $\mathcal{B} \subseteq \{1, \dots, n\}$ to have an unbiased estimation of F as

$$\tilde{F} = \frac{n}{|\mathcal{B}|} \sum_{i \in \mathcal{B}} \left[\log \mathcal{N}(y_i | [\boldsymbol{\mu}_f]_i, [\mathbf{R}_g]_{ii}) - \frac{1}{4} [\boldsymbol{\Sigma}_g]_{ii} - \frac{1}{2} [\boldsymbol{\Sigma}_f \mathbf{R}_g^{-1}]_{ii} \right] - \text{KL}[q(\mathbf{f}_m) | p(\mathbf{f}_m)] - \text{KL}[q(\mathbf{g}_u) | p(\mathbf{g}_u)], \quad (23)$$

where $|\mathcal{B}| \ll n$ is the mini-batch size. More efficiently, since the two variational distributions are defined in terms of KL divergence, we could optimize them along the *natural* gradients instead of the Euclidean gradients, see Appendix C.

Finally, the predictions of stochastic VSHGP (SVSHGP) follow (20a) and (20b), with the predictions of f and g replaced as

$$\begin{aligned} \mu_{f*} &= \mathbf{k}_{*m}^f (\mathbf{K}_{mm}^f)^{-1} \boldsymbol{\mu}_m, \\ \sigma_{f*}^2 &= \mathbf{k}_{**}^f - \mathbf{k}_{*m}^f (\mathbf{K}_{mm}^f)^{-1} (\mathbf{K}_{mm}^f - \boldsymbol{\Sigma}_m) (\mathbf{K}_{mm}^f)^{-1} \mathbf{k}_{m*}^f, \end{aligned}$$

and

$$\begin{aligned} \mu_{g*} &= \mathbf{k}_{*u}^g (\mathbf{K}_{uu}^g)^{-1} (\boldsymbol{\mu}_u - \mu_0 \mathbf{1}) + \mu_0 \mathbf{1}, \\ \sigma_{g*}^2 &= \mathbf{k}_{**}^g - \mathbf{k}_{*u}^g (\mathbf{K}_{uu}^g)^{-1} (\mathbf{K}_{uu}^g - \boldsymbol{\Sigma}_u) (\mathbf{K}_{uu}^g)^{-1} \mathbf{k}_{u*}^g. \end{aligned}$$

Compared to the deterministic VSHGP, the stochastic variant greatly reduces the time complexity from $\mathcal{O}(nm^2 + nu^2)$ to $\mathcal{O}(|\mathcal{B}|m^2 + |\mathcal{B}|u^2 + m^3 + u^3)$, at the cost of requiring many more optimization efforts in the enlarged probabilistic space.⁸ Besides, the capability of SVSHGP akin to VSHGP is still limited to the finite number of global inducing points.

⁸Compared to VSHGP, SVSHGP cannot re-parameterize $\boldsymbol{\mu}_u$ and $\boldsymbol{\Sigma}_u$, and has to infer $m + m(m+1)$ more variational parameters in $\boldsymbol{\mu}_m$ and $\boldsymbol{\Sigma}_m$.

IV. DISTRIBUTED VSHGP

To further improve the *scalability* and *capability* of VSHGP via *many* inducing points, we propose to combine VSHGP with local approximations, e.g., the Bayesian committee machine (BCM) [37], [38]. We particularly care about the capability of VSHGP because of the explicit interaction between f and g in the predictions (17). That means the quality of g in VSHGP affects the prediction mean through (17).

A. Training experts with hybrid parameters

We first partition the training data \mathcal{D} into M subsets $\mathcal{D}_i = \{\mathbf{X}_i, \mathbf{y}_i\}$, $1 \leq i \leq M$. Then, we train a VSHGP expert \mathcal{M}_i on \mathcal{D}_i by using the relevant inducing sets \mathbf{X}_{m_i} and \mathbf{X}_{u_i} . Particularly, to obtain computational gains, an independence assumption is posed for all the experts $\{\mathcal{M}_i\}_{i=1}^M$ such that $\log p(\mathbf{y}; \mathbf{X}, \boldsymbol{\psi})$ is decomposed into the sum of M individuals

$$\log p(\mathbf{y}; \mathbf{X}, \boldsymbol{\psi}) \approx \sum_{i=1}^M \log p(\mathbf{y}_i; \mathbf{X}_i, \boldsymbol{\psi}_i) \geq \sum_{i=1}^M F_{V_i}, \quad (24)$$

where $\boldsymbol{\psi}_i$ is the hyperparameters to be inferred in \mathcal{M}_i , and $F_{V_i} = F(q(\mathbf{g}_{u_i}))$ is the ELBO of \mathcal{M}_i . The factorization in (24) helps efficiently calculate the inversions as $(\mathbf{K}_{mm}^f)^{-1} \approx \text{diag}[\{(\mathbf{K}_{m_i m_i}^f)^{-1}\}_{i=1}^M]$ and $(\mathbf{K}_{mm}^g)^{-1} \approx \text{diag}[\{(\mathbf{K}_{m_i m_i}^g)^{-1}\}_{i=1}^M]$.

We train these VSHGP experts with hybrid parameters. Specifically, the BCM-type aggregation requires sharing the priors $p(f_*)$ and $p(g_*)$ over experts. That means, we should share the hyperparameters including $\boldsymbol{\theta}_f$, $\boldsymbol{\theta}_g$ and μ_0 across experts. These *global* parameters are beneficial for guarding against over-fitting [38], at the cost of however degrading the capability. Hence, we leave the variational parameters $\boldsymbol{\Lambda}_{n_i n_i}$ and the inducing points \mathbf{X}_{m_i} and \mathbf{X}_{u_i} for each expert to infer them individually. These *local* parameters improve capturing local variety by (i) pushing $q(\mathbf{g}_{u_i})$ towards the posterior $p(\mathbf{g}_{u_i} | \mathbf{y}_i)$ of \mathcal{M}_i , and (ii) using many inducing points.

It is notable that because of the local parameters, we should partition the data into *disjoint* experts rather than into *random* experts like [38]. The disjoint partition using clustering techniques produces local and separate experts which are desirable for learning the relevant local parameters. In contrast, the random partition, which assigns points randomly to the subsets, provides global and overlapped experts which are difficult to well estimate the local parameters. For instance, when the distributed DVSHGP (DVSHGP) uses random experts on the toy example below, it fails to capture the heteroscedastic noise.

Finally, suppose that each expert has the same training size $n_0 = n/M$, the training complexity for an expert is $\mathcal{O}(n_0 m_0^2 + n_0 u_0^2)$, where m_0 is the inducing size for \mathbf{f}_i and u_0 the inducing size for \mathbf{g}_i . Due to the M local experts, DVSHGP naturally offers parallel/distributed training, hence reducing the time complexity of VSHGP with a factor ideally close to the number of machines when $m_0 = m$ and $u_0 = u$.

B. Aggregation of experts

For each VSHGP expert \mathcal{M}_i , we obtain the predictive distribution $q_i(y_*)$ with the means $\{\mu_{f_i}(\mathbf{x}_*), \mu_{g_i}(\mathbf{x}_*), \mu_i(\mathbf{x}_*)\}$ and

variances $\{\sigma_{f_i}^2(\mathbf{x}_*), \sigma_{g_i}^2(\mathbf{x}_*), \sigma_i^2(\mathbf{x}_*)\}$. Thereafter, we combine the experts' predictions together to perform the final prediction by, for example the robust BCM (RBCM) aggregation, which naturally supports distributed/parallel computing [38], [57].

The key to the success of aggregation is that we do not directly combine the experts' predictions $\{\mu_i(\mathbf{x}_*), \sigma_i^2(\mathbf{x}_*)\}_{i=1}^M$. This is because (i) the RBCM aggregation of $\{q_i(y_*)\}_{i=1}^M$ produces an invalid prediction variance with increasing n and M [39]; and (ii) the predictive distribution $q_i(y_*)$ in (19) is non-Gaussian. To have a meaningful prediction variance which is crucial for heteroscedastic regression, we perform the RBCM aggregation for the latent functions f and g respectively. This is because the prediction variances of f and g approach zeros with increasing n , which agree with the property of RBCM.

We first have the aggregated prediction for f_* as

$$p_{\mathcal{A}}(f_*|\mathbf{y}, \mathbf{x}_*) = \frac{\prod_{i=1}^M q_i^{\beta_i^f}(f_*)}{p^{\sum_i \beta_i^f - 1}(f_*)}, \quad (25)$$

where the prior $p(f_*) = \mathcal{N}(f_*|0, \sigma_{f^{**}}^2 \triangleq k_{**}^f)$. Hence, the mean and variance are expressed respectively as

$$\mu_{f_{\mathcal{A}}}(\mathbf{x}_*) = \sigma_{f_{\mathcal{A}}}^2(\mathbf{x}_*) \sum_{i=1}^M \beta_i^f \sigma_{f_i}^{-2}(\mathbf{x}_*) \mu_{f_i}(\mathbf{x}_*), \quad (26a)$$

$$\sigma_{f_{\mathcal{A}}}^{-2}(\mathbf{x}_*) = \sum_{i=1}^M \beta_i^f \sigma_{f_i}^{-2}(\mathbf{x}_*) + \left(1 - \sum_{i=1}^M \beta_i^f\right) \sigma_{f^{**}}^{-2}, \quad (26b)$$

where the weight $\beta_i^f \geq 0$ represents the contribution of \mathcal{M}_i at \mathbf{x}_i for f , and is defined as the difference in the differential entropy between the prior $p(f_*)$ and the posterior $q_i(f_*)$ as $\beta_i^f = 0.5(\log \sigma_{f^{**}}^2 - \log \sigma_{f_i}^2(\mathbf{x}_*))$. Similarly, for g which explicitly considers a prior mean μ_0 , the aggregated prediction is

$$p_{\mathcal{A}}(g_*|\mathbf{y}, \mathbf{x}_*) = \frac{\prod_{i=1}^M q_i^{\beta_i^g}(g_*)}{p^{\sum_i \beta_i^g - 1}(g_*)}. \quad (27)$$

Hence, the mean and variance are expressed respectively as

$$\mu_{g_{\mathcal{A}}}(\mathbf{x}_*) = \sigma_{g_{\mathcal{A}}}^2(\mathbf{x}_*) \left[\sum_{i=1}^M \beta_i^g \sigma_{g_i}^{-2}(\mathbf{x}_*) \mu_{g_i}(\mathbf{x}_*) + \left(1 - \sum_{i=1}^M \beta_i^g\right) \sigma_{g^{**}}^{-2} \mu_0 \right], \quad (28a)$$

$$\sigma_{g_{\mathcal{A}}}^{-2}(\mathbf{x}_*) = \sum_{i=1}^M \beta_i^g \sigma_{g_i}^{-2}(\mathbf{x}_*) + \left(1 - \sum_{i=1}^M \beta_i^g\right) \sigma_{g^{**}}^{-2}, \quad (28b)$$

where $\sigma_{g^{**}}^{-2}$ is the prior precision of g , and $\beta_i^g = 0.5(\log \sigma_{g^{**}}^2 - \log \sigma_{g_i}^2(\mathbf{x}_*))$ is the weight of \mathcal{M}_i at \mathbf{x}_i for g .

Thereafter, as shown in Fig. 1, the final prediction mean and variance akin to (20a) and (20b) are respectively combined as

$$\mu_{\mathcal{A}}(\mathbf{x}_*) = \mu_{f_{\mathcal{A}}}(\mathbf{x}_*), \quad (29a)$$

$$\sigma_{\mathcal{A}}^2(\mathbf{x}_*) = \sigma_{f_{\mathcal{A}}}^2(\mathbf{x}_*) + e^{\mu_{g_{\mathcal{A}}}(\mathbf{x}_*) + \sigma_{g_{\mathcal{A}}}^2(\mathbf{x}_*)/2}. \quad (29b)$$

The hierarchical and localized computation structure enables (i) large-scale HGP regression via distributed computations, and (ii) flexible approximation of slow-/quick-varying features

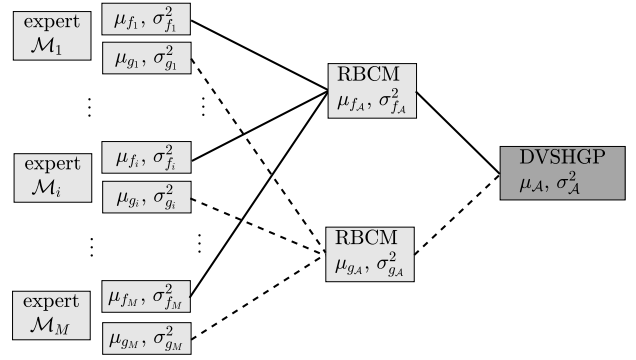


Fig. 1. Hierarchy of the proposed DVSHGP.

by local experts and many inducing points (up to the training size n).

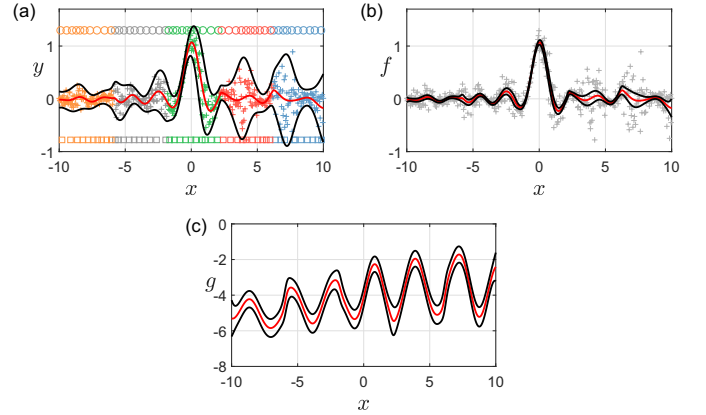


Fig. 2. Illustration of DVSHGP on the toy example. The crosses marked in different colors in (a) represent $M = 5$ subsets. The top circles and bottom squares marked in different colors represent the optimized positions of inducing points for $\{f_i\}_{i=1}^M$ and $\{g_i\}_{i=1}^M$, respectively. The red curves present the prediction mean, whereas the black curves represent 95% confidence interval of the prediction mean.

Finally, we illustrate the DVSHGP on a heteroscedastic toy example expressed as

$$y(x) = \text{sinc}(x) + \epsilon, \quad x \in [-10, 10], \quad (30)$$

where $\epsilon = \mathcal{N}(0, \sigma_\epsilon^2(x))$ and $\sigma_\epsilon(x) = 0.05 + 0.2(1 + \sin(2x))/(1 + e^{-0.2x})$. We draw 500 training points from (30), and use the k -means technique to partition them into five disjoint subsets. We then employ ten inducing points for both f_i and g_i of the VSHGP expert \mathcal{M}_i , $1 \leq i \leq 5$. The modeling results in Fig. 2 turn out that (i) through five local experts, DVSHGP can efficiently employ up to 100 inducing points for modeling, and (ii) DVSHGP successfully describes the underlying function f and the heteroscedastic log noise variance g .

V. DISCUSSIONS

A. Implementation of DVSHGP

Regarding the implementation of DVSHGP, we should infer (i) the global parameters including the kernel parameters θ_f and θ_g , and the mean μ_0 ; and (ii) the local parameters

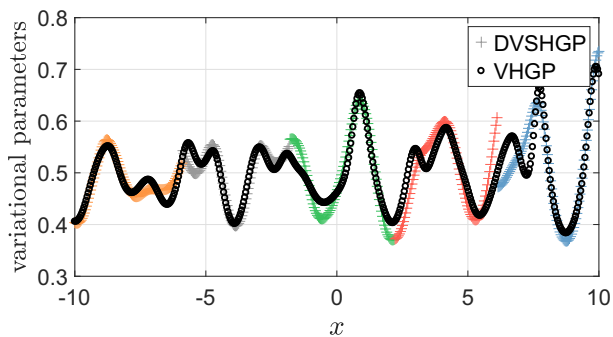


Fig. 3. Illustration of variational parameters learnt respectively by DVSHGP and VHGP on the toy problem. The crosses marked in different colors represent the variational parameters inferred in the five local experts of DVSHGP.

including the variational parameters $\Lambda_{n_i n_i}$ and the inducing parameters \mathbf{X}_{m_i} and \mathbf{X}_{u_i} , for local experts $\{\mathcal{M}_i\}_{i=1}^M$.

Notably, the variational parameters $\Lambda_{n_i n_i}$ are crucial for the success of DVSHGP, since they represent the heteroscedasticity of noise variance. To learn the variational parameters well, there are two issues: (i) how to initialize them and (ii) how to optimize them. As for initialization, let us focus on VSHGP, which is the foundation for the experts in DVSHGP. It is observed in (14a) and (14b) that Λ_{nn} directly determines the initialization of $q(\mathbf{g}_u) = \mathcal{N}(\boldsymbol{\mu}_u, \boldsymbol{\Sigma}_u)$ which approximates $p(\mathbf{g}_u|\mathbf{y})$. Since the prior of \mathbf{g}_u follows $\mathcal{N}(\mathbf{g}_u|\mu_0\mathbf{1}, \mathbf{K}_{uu}^g)$, we intuitively place a prior mean $\mu_0\mathbf{1}$ on $\boldsymbol{\mu}_u$, resulting in $\Lambda_{nn} = 0.5\mathbf{I}$. On the contrary, if we initialize $[\Lambda_{nn}]_{ii}$ with a value larger or smaller than 0.5, the cumulative term $\mathbf{K}_{un}^g(\Lambda_{nn} - 0.5\mathbf{I})\mathbf{1}$ in (14a) becomes far away from zero with increasing n , leading to improper prior mean for $\boldsymbol{\mu}_u$. As for optimization, compared to standard GP, DVSHGP needs to additionally infer n variational parameters and $M(m_0 + u_0)d$ inducing parameters, which greatly enlarge the parameter space and increase the optimization difficulty. Hence, we use an alternating strategy where we first optimize the variational parameters individually to roughly capture the heteroscedasticity, followed by learning all the hyperparameters jointly.

Fig. 3 depicts the inferred variational parameters varying over training points by DVSHGP and the original VHGP [18], respectively, on the toy problem. It turns out that the variational parameters estimated by DVSHGP (i) generally agree with that of VHGP, and (ii) showcase local characteristics that are beneficial for local variety.

B. Implementation of SVSHGP

To effectively infer the variational parameters in $q(\mathbf{f}_m)$ and $q(\mathbf{g}_u)$ through maximizing the ELBO \bar{F} in (23), we adopt the natural gradient descent (NGD), which however should carefully tune the step parameter γ . For the GP regression using Gaussian likelihood, the optimal solution is $\gamma = 1.0$, since taking the unit step is equivalent to performing a variational Bayes update [30]. But for stochastic case, empirical results suggest that the value of γ should be gradually increased to some fixed value. Hence, we follow the schedule in [58]: take $\gamma_{\text{initial}} = 0.0001$ and log-linearly increase γ to $\gamma_{\text{final}} = 0.1$

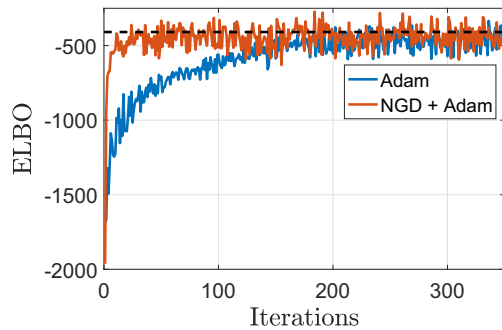


Fig. 4. Illustration of SVSHGP using Adam and NGD+Adam respectively on the toy example. The dash line represents the final ELBO of VSHGP.

over five iterations, and then keep γ_{final} for the remaining iterations.

Thereafter, we employ a hybrid strategy, called NGD+Adam, for optimizing the variational parameters and other hyperparameters simultaneously. Specifically, we perform a step of NGD on variational parameters with aforementioned γ schedule, followed by a step of Adam on the remaining hyperparameters with a fixed step $\gamma_{\text{adam}} = 0.01$.

Fig. 4 depicts the convergence histories of SVSHGP using Adam and NGD+Adam respectively on the toy example (30). We use $m = u = 20$ inducing points and a mini-batch size of $|\mathcal{B}| = 50$. As the ground truth, the final ELBO obtained by VSHGP is also provided. It is observed that (i) the NGD+Adam converges faster than the pure Adam, and (ii) the stochastic optimizers finally approach the solution of VSHGP.

C. DVSHGP vs. (S)VSHGP

Compared to the global (S)VSHGP, the performance of DVSHGP is enhanced by *many* inducing points and localized experts with *individual* variational and inducing parameters, resulting in the capability of capturing quick-varying features. To verify this, we apply DVSHGP and (S)VSHGP to the time-series *solar irradiance* dataset [59] which contains quick-varying and heteroscedastic features.

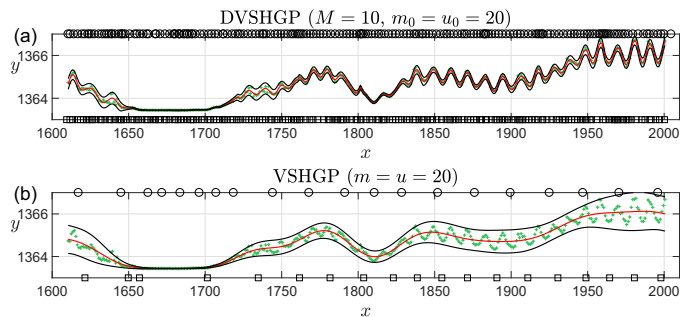


Fig. 5. Comparison of DVSHGP and VSHGP on the *solar irradiance* dataset.

In the comparison, DVSHGP employs the k -means technique to partition the 391 training points into $M = 10$ subsets, and uses $m_0 = u_0 = 20$ inducing points for each expert; (S)VSHGP employs $m = u = 20$ inducing points. Particularly, we initialize the length-scales in the SE kernel (3) as a

pretty small value of 5 for k_f and k_g for (S)VSHGP on this quick-varying dataset. Fig. 5 shows that (i) DVSHGP captures the quick-varying and heteroscedastic features successfully via local experts and many inducing points; (ii) (S)VSHGP however fails due to the small set of global inducing points.⁹

VI. NUMERICAL EXPERIMENTS

This section verifies the proposed DVSHGP and SVSHGP against existing scalable HGPs on a synthetic dataset and four real-world datasets. The comparison includes (i) GPVC [8], (ii) the distributed variant of PIC (dPIC) [29], (iii) FITC [48], and (iv) the SoD based empirical HGP (EHSoD) [11]. Besides, the comparison also employs VSGP [27], a homoscedastic GP which can be used to showcase the benefits brought by the consideration of heteroscedasticity. Finally, we adopt the distributed homoscedastic RBCM model [38], which utilizes all the training data without inducing points, as comparison.

We implement DVSHGP, FITC, EHSoD, VSGP and RBCM based on Rasmussen’s GPML toolbox¹⁰; we implement SVSHGP based on the GPflow package¹¹; we use the published GPVC codes¹² and the dPIC codes¹³. These codes are executed on a personal computer with four 3.70 GHz cores and 16 GB RAM for the synthetic and three medium-sized datasets, and on a Linux workstation with eight 3.20 GHz cores and 32GB memory for the large-scale dataset.

All the GPs employ the SE kernel in (3). Normalization is performed for both \mathbf{X} and \mathbf{y} to have zero mean and unit variance before training. Finally, we use n_* test points $\{\mathbf{X}_*, \mathbf{y}_*\}$ to assess the model accuracy by the standardized mean square error (SMSE) and the mean standardized log loss (MSLL) [1]. SMSE quantifies the discrepancy between the predictions and the exact observations. Particularly, it equals to one when the model always predicts the mean of \mathbf{y} . Moreover, MSLL quantifies the predictive distribution, and is negative for better models. Particularly, it equals to zero when the model always predicts the mean and variance of \mathbf{y} .

A. Synthetic dataset

We herein employ a two dimensional version of the toy example (30) as

$$y(\mathbf{x}) = f(\mathbf{x}) + \epsilon(\mathbf{x}), \quad \mathbf{x} \in [-10, 10]^2,$$

with highly nonlinear latent function $f(\mathbf{x}) = \text{sinc}(0.1x_1x_2)$ and noise $\epsilon(\mathbf{x}) = \mathcal{N}(0, \sigma_\epsilon^2(0.1x_1x_2))$. We randomly generate 10,000 training points and evaluate the model accuracy on 4,900 grid test points. We generate ten instances of the training data such that each model is repeated ten times.

We have $M = 50$ and $m_0 = u_0 = 100$ for DVSHGP, resulting in $n_0 = 200$ data points assigned to each expert; we have $m_b = 300$ basis functions for GPVC; we have $m = 300$ for SVSHGP, FITC and VSGP; we have $m = 300$ and $M =$

50 for dPIC; we have $M = 50$ for RBCM; finally, we train two separate GPs on a subset of size $m_{\text{sod}} = 2,000$ for EHSoD. As for optimization, DVSHGP adopts a two-stage process: it first only optimizes the variational parameters using CGD with up to 30 line searches, and then learns all the parameters jointly using up to 70 line searches; SVSHGP trains with NGD+Adam using $|\beta| = 1,000$ over 1,000 iterations; VSGP, FITC, GPVC and RBCM use CGD with up to 100 line searches to learn the parameters; dPIC employs the default optimization settings in the published codes; and finally EHSoD uses CGD with up to 50 line searches to train the two standard GPs, respectively.

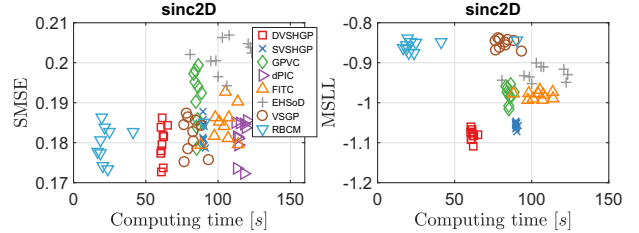


Fig. 6. The performance of different heteroscedastic/homoscedastic GPs over ten runs on the synthetic dataset.

Fig. 6 depicts the modeling results of different models over ten runs on the synthetic *sinc2D* dataset.¹⁴ The horizontal axis represents the sum of training and predicting time for a model. It turns out that DVSHGP, SVSHGP, dPIC, VSGP and RBCM are competitive in terms of SMSE; but DVSHGP and SVSHGP produce better results in terms of MSLL due to well estimated heteroscedastic noise. Compared to the homoscedastic VSGP and RBCM, FITC produces heteroscedastic prediction variances, which is indicated by the lower MSLL, at the cost of (i) sacrificing the prediction mean in terms of SMSE, and (ii) suffering from invalidate noise variance σ_ϵ^2 .¹⁵ As a principled HGP, GPVC performs slightly better than FITC in terms of MSLL. Finally, EHSoD produces the worst SMSE; but due to another separate GP for capturing noise variances, EHSoD outperforms the homoscedastic VSGP and RBCM in terms of MSLL.

In terms of efficiency, RBCM requires less computing time than the others which use approximate inference, because it contains no variational/inducing parameters, resulting in (i) lower complexity, and (ii) early stop for optimization. This also happens for the three datasets below.

Intuitively, Fig. 7 depicts the prediction variances of these GPs except dPIC in comparison to the exact σ^2 on the synthetic dataset. It is first observed that the homoscedastic VSGP and RBCM are unable to describe the complex noise variance by yielding a nearly constant variance over the input domain. In contrast, DVSHGP, SVSHGP and GPVC capture the varying noise variance accurately by using an additional noise process g ; FITC also captures the profile of the exact σ^2 but produces unstable peaks and valleys; EHSoD is found to capture a rough expression of the exact σ^2 .

¹⁴Note that since the dPIC codes only provide the estimation of prediction mean, we did not report its MSLL value as well as the boxplots of noise variance in the following plots.

¹⁵FITC estimates the noise variance σ_ϵ^2 as 0.0030, while VSGP estimates it as 0.0309.

⁹Since VSHGP and SVSHGP show similar predictions on this dataset, we only illustrate the VSHGP predictions in the figure.

¹⁰<http://www.gaussianprocess.org/gpml/code/matlab/doc/>

¹¹<https://github.com/GPflow>

¹²<https://github.com/OxfordML/GPz>

¹³https://github.com/qminh93/dSGP_ICML16

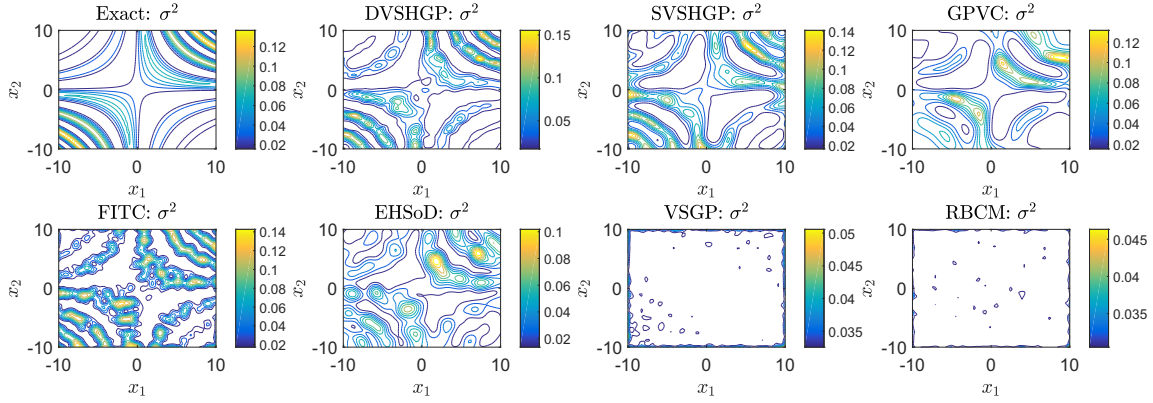


Fig. 7. The exact variance and the prediction variances σ^2 of different heteroscedastic/homoscedastic GPs on the synthetic dataset.

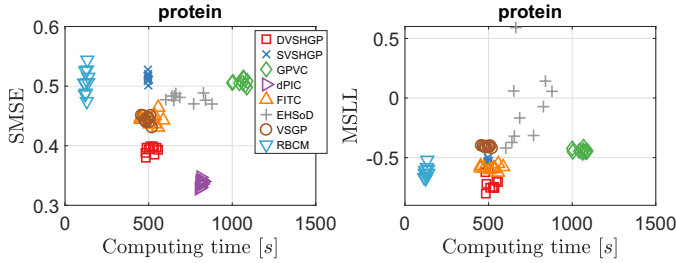


Fig. 8. The performance of different heteroscedastic/homoscedastic GPs over ten runs on the *protein* dataset.

B. Medium real-world datasets

This section conducts comparison on three real-world datasets. The first is the 9D protein dataset [60] with 45,730 data points. This dataset, taken from CASP 5-9, describes the physicochemical properties of protein tertiary structure. The second is the 21D sarcos dataset [1] with 48,933 data points, which relates the inverse kinematics of a robot arm. The third is the 3D *3droad* dataset which comprises 434,874 data points [61] extracted from a 2D road network in North Jutland, Denmark, plussing elevation information.

1) *The protein dataset*: For the *protein* dataset, we randomly choose 35,000 training points and 10,730 test points. In the comparison, we have $M = 100$ (i.e., $n_0 = 350$) and $m_0 = u_0 = 175$ for DVSHGP; we have $m = 400$ for SVSHGP, VSGP and FITC; we have $m = 400$ and $M = 100$ for dPIC; we have $m_b = 400$ for GPVC; we have $M = 100$ for RBCM; and finally we have $m_{\text{sod}} = 4,000$ for EHSoD. As for optimization, SVSHGP trains with NGD+Adam using $|\beta| = 2,000$ over 2,000 iterations. The optimization settings of other GPs keep consistent to that for the synthetic dataset.

The results of different models over ten runs are summarized in Fig. 8. Among the HGPs, it is observed that dPIC outperforms the others in terms of SMSE, followed by DVSHGP. On the other hand, DVSHGP performs the best in terms of MSLL, followed by FITC and SVSHGP. The simple EHSoD is found to produce unstable MSLL results because of the small subset. Finally, as homoscedastic GPs, VSGP and RBCM provide mediocre SMSE and MSLL results.

Next, Fig. 9 offers insights into the distributions of log noise

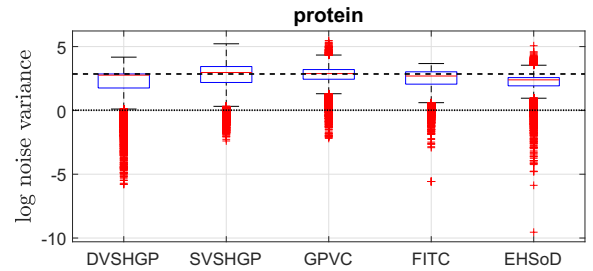


Fig. 9. The distributions of log noise variances of different heteroscedastic/homoscedastic GPs on the *protein* dataset. The dash and dot lines indicate the log noise variances of VSGP and RBCM, respectively.

variances of all the GPs except dPIC on the *protein* dataset for a single run. Note that (i) as homoscedastic GPs, the log noise variances of VSGP and RBCM are marked as dash and dot lines, respectively; and (ii) we plot the variance of $p(f_* | \mathcal{D}, \mathbf{x}_*)$ for FITC since (a) it accounts for the heteroscedasticity and (b) the scalar noise variance σ_ϵ^2 is severely underestimated. The results in Fig. 9 indicate that the *protein* dataset may contain huge noise varying over the input domain. Another observation is that compared to the VSGP using a global inducing set, the localized RBCM provides a more compact estimation of σ_ϵ^2 . This compact noise variance, which has also been observed on the two datasets below, brings lower MSLL for RBCM.

Furthermore, we clearly see the interaction between f and g for DVSHGP, SVSHGP and GPVC. The small MSLL of RBCM suggests that the *protein* dataset may own small noise variances at some test points. Hence, the localized DVSHGP, which is enabled to capture the local variety through *individual* variational and inducing parameters for each expert, produces a longer tail in Fig. 9. The well estimated heteroscedastic noise in turn improves the prediction mean of DVSHGP through the interaction between f and g . In contrast, due to the limited global inducing set, the prediction mean of SVSHGP and GPVC is traded for capturing heteroscedastic noise.

Notably, the performance of sparse GPs is affected by their modeling parameters, e.g., the inducing sizes m_0 , m , u_0 and u , the number of basis functions m_b , and the subset size m_{sod} . Fig. 10(a) and (b) depict the average results of sparse GPs over ten runs using different parameters. Particularly,

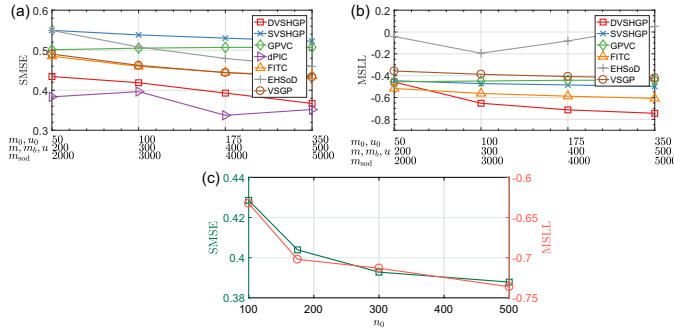


Fig. 10. The effect of algorithmic parameters on the performance of different sparse GPs on the *protein* dataset.

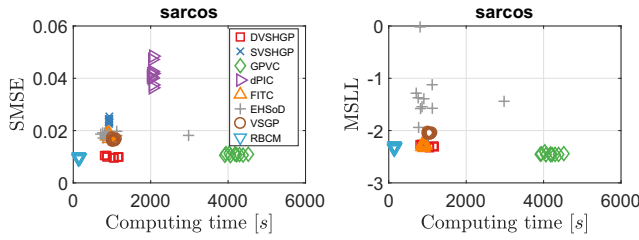


Fig. 11. The performance of different heteroscedastic/homoscedastic GPs over ten runs on the *sarcos* dataset.

we investigate the impact of subset size n_0 on DVSHGP in Fig. 10(c) using $m_0 = u_0 = 0.5n_0$. It is found that DVSHGP favours large n_0 (small M) and large m_0 and u_0 . Similarly, VSGP and FITC favour more inducing points. However, dPIC offers an unstable SMSE performance with increasing m . GPVC performs slightly worse with increasing m_b in terms of both SMSE and MSLL, which has also been observed in the original paper [8]. This may be caused by the sharing of basis functions for f and g . Finally, because of the difficulty of approximating the empirical variances, EHSod showcases poor MSLL values when $m_{sod} \geq 3000$.

2) *The sarcos dataset*: For the *sarcos* dataset, we randomly choose 40,000 training points and 8,933 test points. In the comparison, we have $M = 120$ (i.e., $n_0 \approx 333$) and $m_0 = u_0 = 175$ for DVSHGP; we have $m = 600$ for SVSHGP, VSGP and FITC; we have $m = 600$ and $M = 120$ for dPIC; we have $m_b = 600$ for GPVC; we have $M = 120$ for RBCM; and finally we have $m_{sod} = 4,000$ for EHSod. The optimization settings are the same as before.

The results of different models over ten runs on the *sarcos* dataset are depicted in Fig. 11. Besides, Fig. 12 depicts the log noise variances of the GPs on this dataset. Different from the *protein* dataset, the *sarcos* dataset seems to have weak heteroscedastic noises across the input domain, which is verified by the facts that (i) the noise variance of DVSHGP is a constant, and (ii) DVSHGP agrees with RBCM in terms of both SMSE and MSLL. Hence, all the HGPs except EHSod perform similarly in terms of MSLL, and most of the EHSod runs produce negative values.

In addition, the weak heteroscedasticity in the *sarcos* dataset reveals that we can use only a few inducing points for g to speed up the inference. For instance, we retrain DVSHGP using the same parameters except for $u_0 = 5$. This extremely

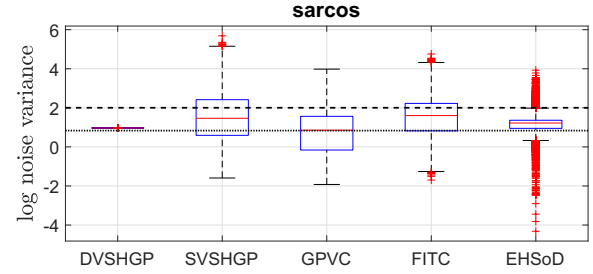


Fig. 12. The distributions of log noise variances of different heteroscedastic/homoscedastic GPs on the *sarcos* dataset. The dash and dot lines indicate the log noise variances of VSGP and RBCM, respectively.

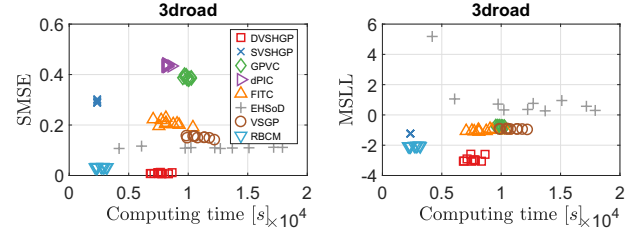


Fig. 13. The performance of different heteroscedastic/homoscedastic GPs over ten runs on the *3droad* dataset.

small inducing set for g brings (i) much less computing time of about 350 s, and (ii) almost the same model accuracy with SMSE = 0.0099 and MSLL = -2.3034.

3) *The 3droad dataset*: Finally, for the *3droad* dataset, we randomly choose 390,000 training points, and use the remaining 44,874 data points for testing. In the comparison, we have $M = 800$ (i.e., $n_0 \approx 487$) and $m_0 = u_0 = 250$ for DVSHGP; we have $m = 500$ for SVSHGP, VSGP and FITC; we have $m = 500$ and $M = 800$ for dPIC; we have $m_b = 500$ for GPVC; we have $M = 800$ for RBCM; and finally we have $m_{sod} = 8,000$ for EHSod. As for optimization, SVSHGP trains with NGD+Adam using $|\mathcal{B}| = 4,000$ over 4,000 iterations. The optimization settings of other GPs keep the same as before.

The results of different models over ten runs on the *3droad* dataset are depicted in Fig. 13. It is observed that DVSHGP outperforms the others in terms of both SMSE and MSLL, followed by RBCM. For other HGPs, especially SVSHGP and GPVC, the relatively poor noise variance (large MSLL) in turn sacrifices the accuracy of prediction mean. Even though, the heteroscedastic noise helps SVSHGP, GPVC and FITC produce MSLL similar to that of VSGP.

In addition, Fig. 14 depicts the log noise variances of these GPs on the *3droad* dataset. The highly accurate prediction mean of DVSHGP helps well estimate the heteroscedastic noise. It is observed that (i) the noise variances estimated by DVSHGP are more compact than that of other HGPs; and (ii) the average noise variance agrees with that of RBCM.

Finally, the results from the *3droad* dataset together with the other two datasets indicate that:

- the well estimated noise variance of HGPs will in turn improve the prediction mean via the interaction between f and g ; otherwise, it may sacrifice the prediction mean;

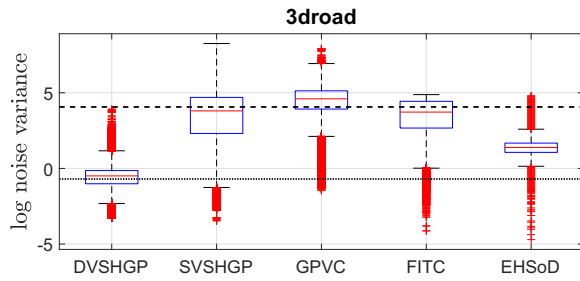


Fig. 14. The distributions of log noise variances of different heteroscedastic/homoscedastic GPs on the *3droad* dataset. The dash and dot lines indicate the log noise variances of VSGP and RBCM, respectively.

- the heteroscedastic noise usually improves scalable HGPs over the homoscedastic VSGP in terms of MSLL.

C. Large real-world dataset

The final section evaluates the performance of different GPs on the 11D electric dataset,¹⁶ which is partitioned into two million training points and 49,280 test points. The scalable HGPs in the comparison include DVSHGP, SVSHGP, dPIC and EHSoD.¹⁷ Besides, the RBCM and the stochastic variant of VSGP, named SVGP [30], are employed for comparison.

In the comparison, we have $M = 2,000$ (i.e., $n_0 = 1,000$) and $m_0 = u_0 = 300$ for DVSHGP; we have $m = 2,500$ for SVSHGP and SVGP; we have $m = 2,500$ and $M = 2,000$ for dPIC; we have $M = 2,000$ for RBCM; and finally we have $m_{\text{sod}} = 15,000$ for EHSoD. As for optimization, SVSHGP trains with NGD+Adam using $|\mathcal{B}| = 5,000$ over 10,000 iterations; The optimization settings of other GPs keep the same as before.

The average results over five runs in Table I indicate that DVSHGP outperforms the others in terms of both SMSE and MSLL, followed by SVSHGP. The simple EHSoD provides the worst performance, and cannot be improved by using larger m_{sod} due to the memory limit in current infrastructure. Additionally, in terms of efficiency, we find that (i) SVSHGP is better than DVSHGP due to the parallel/GPU acceleration deployed in Tensorflow;¹⁸ (ii) SVGP is better than SVSHGP because of lower complexity; and (iii) the huge computing time of dPIC might be incurred by the unoptimized codes.

Finally, due to the distributed framework, Fig. 15(a) depicts the total computing time of DVSHGP using different numbers of processing cores. It is observed that the DVSHGP using eight cores achieves a speedup around 3.5 in comparison to the centralized counterpart. Fig. 15(b) also exploits the performance of SVSHGP using a varying mini-batch size $|\mathcal{B}|$. It is observed that (i) a small $|\mathcal{B}|$ significantly speeds up the model training, and (ii) different mini-batch sizes yield similar SMSE and MSLL here, because the model has been optimized over sufficient iterations.

¹⁶The dataset is available at <https://archive.ics.uci.edu/ml/index.php>.

¹⁷GPVC and FITC are unaffordable for this massive dataset. Besides, the stochastic variant of FITC in [31] is not included, since it does not provide an end-to-end training.

¹⁸Further GPU speedup could be utilized for DVSHGP in the Matlab environment.

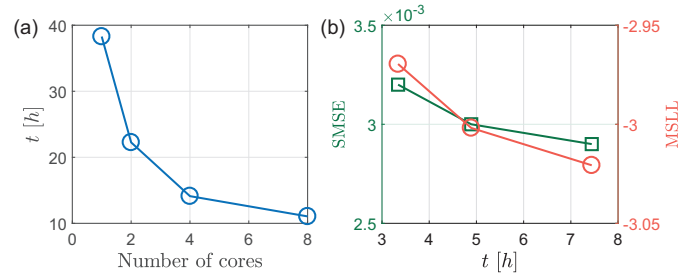


Fig. 15. Illustration of (a) the computing time of DVSHGP vs. number of processing cores, and (b) the performance of SVSHGP, from left to right, using $|\mathcal{B}| = 1,000, 2,500$ and $5,000$ on the *electric* dataset.

VII. CONCLUSIONS

In order to scale up HGP to large-scale datasets, we have presented distributed and stochastic variational sparse HGPs. The proposed SVSHGP improves the scalability through stochastic variational inference. The proposed DVSHGP (i) enables large-scale HGP regression via distributed computations, and (ii) achieves high model capability via localized experts and many inducing points. We compare them to state-of-the-art scalable homoscedastic/heteroscedastic GPs on a synthetic dataset and four real-world datasets. The comparative results obtained indicate that DVSHGP exhibits superior performance in terms of both SMSE and MSLL; while due to the limited global inducing set, SVSHGP may sacrifice the prediction mean for capturing heteroscedastic noise.

Our future work will consider the heteroscedasticity in the underlying function f , i.e., the non-stationary, like [17], [24], [41]. The integration of various kinds of heteroscedasticity is believed to improve predictions.

APPENDIX A

NON-NEGATIVITY OF Λ_{nn}

We know that the variational diagonal matrix Λ_{nn} expresses

$$\Lambda_{nn} = 0.5(\Lambda_{nn}^a + \Lambda_{nn}^b + \mathbf{I}).$$

In order to prove the non-negativity of Λ_{nn} , we should figure out the non-negativity of the diagonal elements of $\Lambda_{nn}^a + \mathbf{I}$ and Λ_{nn}^b , respectively.

Firstly, the diagonal elements of Λ_{nn}^b write

$$[\Lambda_{nn}^b]_{ii} = [(\mathbf{K}_{nn}^f - \mathbf{Q}_{nn}^f)\mathbf{R}_g^{-1}]_{ii}, \quad 1 \leq i \leq n,$$

where the diagonal elements of \mathbf{R}_g^{-1} satisfy $[\mathbf{R}_g^{-1}]_{ii} = e^{[\Sigma_g]_{ii}/2 - [\mu_g]_i} > 0$, $1 \leq i \leq n$; and the diagonal elements of $\mathbf{K}_{nn}^f - \mathbf{Q}_{nn}^f$ are the variances of training conditional $p(\mathbf{f}|\mathbf{f}_m)$. Therefore, Λ_{nn}^b has non-negative diagonal elements.

Secondly, the diagonal elements of $\Lambda_{nn}^a + \mathbf{I}$ write, given $\beta_n = \Sigma_y^{-1}\mathbf{y}$,

$$[\Lambda_{nn}^a + \mathbf{I}]_{ii} = [\beta_n \beta_n^\top \mathbf{R}_g - \Sigma_y^{-1} \mathbf{R}_g + \mathbf{I}]_{ii}, \quad 1 \leq i \leq n.$$

For $\beta_n \beta_n^\top \mathbf{R}_g$, the diagonal elements are non-negative. For $\mathbf{I} - \Sigma_y^{-1} \mathbf{R}_g$, given the Cholesky decomposition $\mathbf{K}_\Lambda^f = \mathbf{L}_\Lambda^f (\mathbf{L}_\Lambda^f)^\top$, we have

$$\begin{aligned} \mathbf{I} - \Sigma_y^{-1} \mathbf{R}_g &= [\mathbf{R}_g^{-1} \mathbf{K}_{nm}^f (\mathbf{K}_\Lambda^f)^{-1} \mathbf{K}_{mn}^f \mathbf{R}_g^{-1}] \mathbf{R}_g \\ &= [\mathbf{R}_g^{-1} \mathbf{K}_{nm}^f (\mathbf{L}_\Lambda^f)^{-\top} (\mathbf{L}_\Lambda^f)^{-1} \mathbf{K}_{mn}^f \mathbf{R}_g^{-1}] \mathbf{R}_g, \end{aligned}$$

TABLE I
COMPARISON ON THE *electric* DATASET IN TERMS OF SMSE, MSLL AND COMPUTING TIME t .

	DVSHGP	SVSHGP	dPIC	EHS _{oD}	SVGP	RBCM
SMSE	0.0020	0.0029	0.0042	0.0103	0.0028	0.0023
MSLL	-3.4456	-3.1207	-	-1.9453	-2.8489	-3.0647
t [h]	11.05	7.44	47.22	4.72	3.55	3.97

indicating that the diagonal elements must be non-negative.

Hence, from the foregoing discussions, we know that Λ_{nn} is a non-negative diagonal matrix.

APPENDIX B

DERIVATIVES OF F_V W.R.T. HYPERPARAMETERS

Let $\lambda_n = \log(\Lambda_{nn}\mathbf{1})$ collects n variational parameters in the log form for non-negativity, we have the derivatives of F_V w.r.t. λ_n as

$$\frac{\partial F_V}{\partial \lambda_n} = \Lambda_{nn} \left[\frac{1}{2}(\mathbf{Q}_{nn}^g + \frac{1}{2}\mathbf{A}_{nn})\Lambda_{nn}^{ab}\mathbf{1} + \frac{1}{4}\mathbf{A}_{nn}\mathbf{1} - \frac{1}{2}\mathbf{A}_{nn}\Lambda_{nn}\mathbf{1} - \mu_g + \mu_0\mathbf{1} \right],$$

where $\mathbf{A}_{nn} = (\mathbf{K}_{nu}^g \mathbf{K}_{\Lambda}^{-1} \mathbf{K}_{un}^g)^{\odot 2}$, and the operator $\odot 2$ represents the element-wise power.

The derivatives of F_V w.r.t. the kernel parameters $\theta_f = \{\theta_i^f\}$ are

$$\frac{\partial F_V}{\partial \theta_i^f} = \frac{1}{2} \text{Tr} \left[(\beta_n \beta_n^\top - \Sigma_y^{-1} + \mathbf{R}_g^{-1}) \frac{\partial \mathbf{Q}_{nn}^f}{\partial \theta_i^f} - \mathbf{R}_g^{-1} \frac{\partial \mathbf{K}_{nn}^f}{\partial \theta_i^f} \right],$$

where

$$\frac{\partial \mathbf{Q}_{nn}^f}{\partial \theta_i^f} = \Omega_{nu}^f \frac{\partial \mathbf{K}_{un}^f}{\partial \theta_i^f} + \frac{\partial \mathbf{K}_{nu}^f}{\partial \theta_i^f} (\Omega_{nu}^f)^\top - \Omega_{nu}^f \frac{\partial \mathbf{K}_{uu}^f}{\partial \theta_i^f} (\Omega_{nu}^f)^\top.$$

The derivatives of F_V w.r.t. the kernel parameters $\theta_g = \{\theta_i^g\}$ are

$$\frac{\partial F_V}{\partial \theta_i^g} = \frac{1}{2} \text{Tr} \left[\frac{\partial \mu_g}{\partial \theta_i^g} (\mathbf{1}^\top \Lambda_{nn}) - \frac{1}{2} (\Lambda_{nn} + \mathbf{I}) \frac{\partial \Sigma_g}{\partial \theta_i^g} \right] - \frac{1}{2} \text{Tr} \left[\mathbf{V}_{uu}^g \frac{\partial \mathbf{K}_{uu}^g}{\partial \theta_i^g} - (\Omega_{nu}^g)^\top \Lambda_{nn} \Omega_{nu}^g \frac{\partial \Sigma_u}{\partial \theta_i^g} + 2 \frac{\partial \mu_u}{\partial \theta_i^g} \gamma_u \right],$$

where $\gamma_u = (\mathbf{K}_{uu}^g)^{-1}(\mu_u - \mu_0\mathbf{1})$, $\mathbf{V}_{uu}^g = (\mathbf{K}_{uu}^g)^{-1} - \gamma_u \gamma_u^\top - (\mathbf{K}_{uu}^g)^{-1} \Sigma_u (\mathbf{K}_{uu}^g)^{-1}$, and the pre-calculated derivatives are expressed as, given $\Omega_{nu}^\Lambda = \mathbf{K}_{nu}^\Lambda \mathbf{K}_{\Lambda}^{-1}$,

$$\begin{aligned} \frac{\partial \mathbf{K}_{\Lambda}}{\partial \theta_i^g} &= \frac{\partial \mathbf{K}_{uu}^g}{\partial \theta_i^g} + \frac{\partial \mathbf{K}_{un}^g}{\partial \theta_i^g} \Lambda_{nn} \mathbf{K}_{nu}^g + \mathbf{K}_{un}^g \Lambda_{nn} \frac{\partial \mathbf{K}_{nu}^g}{\partial \theta_i^g}, \\ \frac{\partial \Sigma_g}{\partial \theta_i^g} &= \frac{\partial \mathbf{K}_{nn}^g}{\partial \theta_i^g} - \frac{\partial \mathbf{Q}_{nn}^g}{\partial \theta_i^g} + \frac{\partial \mathbf{K}_{nu}^g}{\partial \theta_i^g} (\Omega_{nu}^\Lambda)^\top + \Omega_{nu}^\Lambda \frac{\partial \mathbf{K}_{un}^g}{\partial \theta_i^g} \\ &\quad - \Omega_{nu}^\Lambda \frac{\partial \mathbf{K}_{\Lambda}}{\partial \theta_i^g} (\Omega_{nu}^\Lambda)^\top, \\ \frac{\partial \Sigma_u}{\partial \theta_i^g} &= \mathbf{K}_{uu}^g \mathbf{K}_{\Lambda}^{-1} \frac{\partial \mathbf{K}_{uu}^g}{\partial \theta_i^g} + \frac{\partial \mathbf{K}_{uu}^g}{\partial \theta_i^g} \mathbf{K}_{\Lambda}^{-1} \mathbf{K}_{uu}^g \\ &\quad - \mathbf{K}_{uu}^g \mathbf{K}_{\Lambda}^{-1} \frac{\partial \mathbf{K}_{\Lambda}}{\partial \theta_i^g} \mathbf{K}_{\Lambda}^{-1} \mathbf{K}_{uu}^g, \\ \frac{\partial \mu_g}{\partial \theta_i^g} &= \frac{\partial \mathbf{Q}_{nn}^g}{\partial \theta_i^g} (\Lambda_{nn} - \frac{1}{2}\mathbf{I})\mathbf{1}, \\ \frac{\partial \mu_u}{\partial \theta_i^g} &= \frac{\partial \mathbf{K}_{un}^g}{\partial \theta_i^g} (\Lambda_{nn} - \frac{1}{2}\mathbf{I})\mathbf{1}. \end{aligned}$$

The derivatives of F_V w.r.t. the mean parameter μ_0 of g is

$$\frac{\partial F_V}{\partial \mu_0} = \frac{1}{2} \text{Tr}(\Lambda_{nn}^{ab}).$$

Finally, we obtain the derivatives of F_V w.r.t. the inducing points \mathbf{X}_m and \mathbf{X}_u . By regarding the inducing points as parameters in the covariance matrices, we get the derivatives $\partial \mathbf{K}_{nm}^f / \partial t_{ij}^f$, $\partial \mathbf{K}_{mn}^f / \partial t_{ij}^f$, $\partial \mathbf{K}_{mm}^f / \partial t_{ij}^f$, $\partial \mathbf{K}_{nu}^g / \partial t_{ij}^g$, $\partial \mathbf{K}_{un}^g / \partial t_{ij}^g$, and $\partial \mathbf{K}_{uu}^g / \partial t_{ij}^g$, where $t_{ij}^f = [\mathbf{X}_m]_{ij}$ and $t_{ij}^g = [\mathbf{X}_u]_{ij}$. We first obtain the derivatives of F w.r.t. \mathbf{X}_m as

$$\frac{\partial F_V}{\partial t_{ij}^f} = 2 \text{Tr} \left[\frac{\partial \mathbf{K}_{nm}^f}{\partial t_{ij}^f} \mathbf{A}_{mn}^f \right] + \text{Tr} \left[\frac{\partial \mathbf{K}_{mm}^f}{\partial t_{ij}^f} \mathbf{A}_{mm}^f \right],$$

where $\mathbf{A}_{mn}^f = 0.5(\Omega_{nm}^f)^\top (\beta_n \beta_n^\top - \Sigma_y^{-1} + \mathbf{R}_g^{-1})$, and $\mathbf{A}_{mm}^f = -\mathbf{A}_{mn}^f \Omega_{nm}^f$. Similarly, the derivatives of F_V w.r.t. \mathbf{X}_u write

$$\frac{\partial F_V}{\partial t_{ij}^g} = \text{Tr} \left[\frac{\partial \mathbf{K}_{nu}^g}{\partial t_{ij}^g} \mathbf{A}_{un}^g \right] + \text{Tr} \left[\mathbf{A}_{nu}^g \frac{\partial \mathbf{K}_{un}^g}{\partial t_{ij}^g} \right] + \text{Tr} \left[\frac{\partial \mathbf{K}_{uu}^g}{\partial t_{ij}^g} \mathbf{A}_{uu}^g \right].$$

For \mathbf{A}_{un}^g in $\partial F_V / \partial t_{ij}^g$, we have

$$\begin{aligned} \mathbf{A}_{un}^g &= \underbrace{0.5(\Omega_{nu}^g)^\top (\Lambda_{nn} - 0.5\mathbf{I})\mathbf{1}(\mathbf{1}^\top \Lambda_{nn}^{ab})}_{\mathbf{T}_1} \\ &\quad + \underbrace{0.25(\mathbf{H}_{uu} \mathbf{K}_{un}^g \Lambda_{nn} - [\Omega_{nu}^\Lambda + \Omega_{nu}^g]^\top (\Lambda_{nn}^{ab} + \mathbf{I}))}_{\mathbf{T}_2} \\ &\quad + \underbrace{0.5(\mathbf{J}_{uu} \mathbf{K}_{un}^g \Lambda_{nn} - \gamma_u \mathbf{1}^\top (\Lambda_{nn} - 0.5\mathbf{I}))}_{\mathbf{T}_3}. \end{aligned}$$

where $\mathbf{H}_{uu} = (\Omega_{nu}^\Lambda)^\top (\Lambda_{nn}^{ab} + \mathbf{I}) \Omega_{nu}^\Lambda$, and $\mathbf{J}_{uu} = \mathbf{K}_{\Lambda}^{-1} \mathbf{K}_{uu}^g ((\mathbf{K}_{uu}^g)^{-1} - \Sigma_u^{-1}) \mathbf{K}_{uu}^g \mathbf{K}_{\Lambda}^{-1}$. For \mathbf{A}_{nu}^g , we have

$$\mathbf{A}_{nu}^g = 0.5(\Lambda_{nn} - 0.5\mathbf{I})\mathbf{1}(\mathbf{1}^\top \Lambda_{nn}^{ab}) \Omega_{nu}^g + \mathbf{T}_2^\top + \mathbf{T}_3^\top.$$

For \mathbf{A}_{uu}^g , we have

$$\begin{aligned} \mathbf{A}_{uu}^g &= -\mathbf{T}_1 \Omega_{nu}^g - 0.25((\Omega_{nu}^g)^\top (\Lambda_{nn}^{ab} + \mathbf{I}) \Omega_{nu}^g - \mathbf{H}_{uu}) \\ &\quad + 0.5(\mathbf{P}_{uu} + \mathbf{P}_{uu}^\top + \mathbf{V}_{uu}^g - \mathbf{J}_{uu}), \end{aligned}$$

where $\mathbf{P}_{uu} = \mathbf{K}_{\Lambda}^{-1} \mathbf{K}_{uu}^g ((\mathbf{K}_{uu}^g)^{-1} - \Sigma_u^{-1})$.

The calculation of $\partial F_V / \partial t_{ij}^f$ and $\partial F_V / \partial t_{ij}^g$ requires a loop over $m \times d$ and $u \times d$ parameters of the inducing points, which is quite slow for even moderate m , u and d . Fortunately, we know that the derivative $\partial \mathbf{K} / \partial t_{ij}$ only has n or m (u) non-zero elements. Due to the sparsity, $\partial \mathbf{K} / \partial t_{ij}$ can be performed in vectorized operations such that the derivatives w.r.t. all the inducing points can be calculated along a specific dimension.

APPENDIX C

NATURAL GRADIENTS OF $q(\mathbf{f}_m)$ AND $q(\mathbf{g}_u)$

For exponential family distributions¹⁹ parameterized by natural parameters $\boldsymbol{\theta}$, we update the parameters using natural gradients as

$$\boldsymbol{\theta}_{(t+1)} = \boldsymbol{\theta}_{(t)} - \gamma_{(t)} \mathbf{G}_{\boldsymbol{\theta}_{(t)}}^{-1} \frac{\partial F}{\partial \boldsymbol{\theta}_{(t)}} = \boldsymbol{\theta}_{(t)} - \gamma_{(t)} \frac{\partial F}{\partial \boldsymbol{\psi}_{(t)}},$$

where F is the objective function, and $\mathbf{G}_{\boldsymbol{\theta}} == \partial \boldsymbol{\psi}_{(t)} / \partial \boldsymbol{\theta}_{(t)}$ is the fisher information matrix with $\boldsymbol{\psi}$ being the expectation parameters of exponential distributions.

For $q(\mathbf{g}_u) \sim \mathcal{N}(\mathbf{g}_u | \boldsymbol{\mu}_u, \boldsymbol{\Sigma}_u)$, its natural parameters are $\boldsymbol{\theta}$ which are partitioned into two components

$$\boldsymbol{\theta}_1 = \boldsymbol{\Sigma}_u^{-1} \boldsymbol{\mu}_u, \quad \boldsymbol{\Theta}_2 = -\frac{1}{2} \boldsymbol{\Sigma}_u^{-1},$$

where $\boldsymbol{\theta}_1$ comprises the first m elements of $\boldsymbol{\theta}$, and $\boldsymbol{\Theta}_2$ the remaining elements reshaped to a square matrix. Accordingly, the expectation parameters $\boldsymbol{\psi}$ are divided as

$$\boldsymbol{\psi}_1 = \boldsymbol{\mu}_u, \quad \boldsymbol{\Psi}_2 = \boldsymbol{\mu}_u \boldsymbol{\mu}_u^T + \boldsymbol{\Sigma}_u.$$

Thereafter, we update the natural parameters with step $\gamma_{(t)}$ as

$$\boldsymbol{\theta}_{1(t+1)} = \boldsymbol{\Sigma}_{u(t)}^{-1} \boldsymbol{\mu}_{u(t)} - \gamma_{(t)} \frac{\partial F}{\partial \boldsymbol{\psi}_{1(t)}},$$

$$\boldsymbol{\Theta}_{2(t+1)} = -\frac{1}{2} \boldsymbol{\Sigma}_{u(t)}^{-1} - \gamma_{(t)} \frac{\partial F}{\partial \boldsymbol{\Psi}_{2(t)}},$$

where $\partial F / \partial \boldsymbol{\psi}_{1(t)} = \partial F / \partial \boldsymbol{\mu}_{u(t)}$ and $\partial F / \partial \boldsymbol{\Psi}_{2(t)} = \partial F / \partial \boldsymbol{\Sigma}_{u(t)}$. The derivatives $\partial F / \partial \boldsymbol{\mu}_u$ and $\partial F / \partial \boldsymbol{\Sigma}_u$ are respectively expressed as

$$\frac{\partial F}{\partial \boldsymbol{\mu}_u} = \frac{1}{2} (\boldsymbol{\Omega}_{nu}^g)^T \boldsymbol{\Lambda}_{nn}^{a'b} \mathbf{1} - (\mathbf{K}_{uu}^g)^{-1} (\boldsymbol{\mu}_u - \boldsymbol{\mu}_0 \mathbf{1}),$$

$$\frac{\partial F}{\partial \boldsymbol{\Sigma}_u} = -\frac{1}{4} (\boldsymbol{\Omega}_{nu}^g)^T (\boldsymbol{\Lambda}_{nn}^{a'b} + \mathbf{I}) \boldsymbol{\Omega}_{nu}^g + \frac{1}{2} [\boldsymbol{\Sigma}_u^{-1} - (\mathbf{K}_{uu}^g)^{-1}],$$

where $\boldsymbol{\Lambda}_{nn}^{a'b} = \boldsymbol{\Lambda}_{nn}^{a'} + \boldsymbol{\Lambda}_{nn}^b$, and $\boldsymbol{\Lambda}_{nn}^{a'}$ is a diagonal matrix with the diagonal element being

$$[\boldsymbol{\Lambda}_{nn}^{a'}]_{ii} = [\mathbf{R}_g^{-1} (\mathbf{y} - \boldsymbol{\Omega}_{nm}^f \boldsymbol{\mu}_m) (\mathbf{y} - \boldsymbol{\Omega}_{nm}^f \boldsymbol{\mu}_m)^T - \mathbf{I}]_{ii}.$$

For $q(\mathbf{f}_m) \sim \mathcal{N}(\mathbf{f}_m | \boldsymbol{\mu}_m, \boldsymbol{\Sigma}_m)$, the updates of $\boldsymbol{\mu}_{m(t+1)}$ and $\boldsymbol{\Sigma}_{m(t+1)}$ follow the foregoing steps, with the derivatives $\partial F / \partial \boldsymbol{\mu}_m$ and $\partial F / \partial \boldsymbol{\Sigma}_m$ taking (22).

ACKNOWLEDGMENT

This work was conducted within the Rolls-Royce@NTU Corporate Lab with support from the National Research Foundation (NRF) Singapore under the Corp Lab@University Scheme. It is also partially supported by the Data Science and Artificial Intelligence Research Center (DSAIR) and the School of Computer Science and Engineering at Nanyang Technological University.

¹⁹The PDF of exponential family is $p(\mathbf{x}) = h(\mathbf{x}) e^{\boldsymbol{\theta}^T \mathbf{t}(\mathbf{x}) - A(\boldsymbol{\theta})}$, where $\boldsymbol{\theta}$ is natural parameters, $h(\mathbf{x})$ is underlying measure, $\mathbf{t}(\mathbf{x})$ is sufficient statistic, and $A(\boldsymbol{\theta})$ is log normalizer. Besides, the expectation parameters are defined as $\boldsymbol{\psi} = \mathbb{E}_{p(\mathbf{x})}[\mathbf{t}(\mathbf{x})]$.

REFERENCES

- [1] C. E. Rasmussen and C. K. I. Williams, *Gaussian processes for machine learning*. MIT Press, 2006.
- [2] N. Lawrence, "Probabilistic non-linear principal component analysis with Gaussian process latent variable models," *Journal of Machine Learning Research*, vol. 6, no. Nov, pp. 1783–1816, 2005.
- [3] B. Shahriari, K. Swersky, Z. Wang, R. P. Adams, and N. De Freitas, "Taking the human out of the loop: A review of Bayesian optimization," *Proceedings of the IEEE*, vol. 104, no. 1, pp. 148–175, 2016.
- [4] H. Liu, J. Cai, and Y. Ong, "Remarks on multi-output Gaussian process regression," *Knowledge-Based Systems*, vol. 144, no. March, pp. 102–121, 2018.
- [5] B. Settles, "Active learning," *Synthesis Lectures on Artificial Intelligence and Machine Learning*, vol. 6, no. 1, pp. 1–114, 2012.
- [6] P. Kou, D. Liang, L. Gao, and J. Lou, "Probabilistic electricity price forecasting with variational heteroscedastic Gaussian process and active learning," *Energy Conversion and Management*, vol. 89, pp. 298–308, 2015.
- [7] M. Lázaro-Gredilla, M. K. Titsias, J. Verrelst, and G. Camps-Valls, "Retrieval of biophysical parameters with heteroscedastic Gaussian processes," *IEEE Geoscience and Remote Sensing Letters*, vol. 11, no. 4, pp. 838–842, 2014.
- [8] I. A. Almosallam, M. J. Jarvis, and S. J. Roberts, "GPz: non-stationary sparse Gaussian processes for heteroscedastic uncertainty estimation in photometric redshifts," *Monthly Notices of the Royal Astronomical Society*, vol. 462, no. 1, pp. 726–739, 2016.
- [9] M. Bauza and A. Rodriguez, "A probabilistic data-driven model for planar pushing," in *ICRA*, 2017, pp. 3008–3015.
- [10] A. J. Smith, M. AlAbsi, and T. Fields, "Heteroscedastic Gaussian process-based system identification and predictive control of a quadcopter," in *2018 AIAA Atmospheric Flight Mechanics Conference*, 2018, p. 0298.
- [11] S. Urban, M. Ludersdorfer, and P. Van Der Smagt, "Sensor calibration and hysteresis compensation with heteroscedastic Gaussian processes," *IEEE Sensors Journal*, vol. 15, no. 11, pp. 6498–6506, 2015.
- [12] F. C. Pereira, C. Antoniou, J. A. Fargas, and M. Ben-Akiva, "A metamodel for estimating error bounds in real-time traffic prediction systems," *IEEE Transactions on Intelligent Transportation Systems*, vol. 15, no. 3, pp. 1310–1322, 2014.
- [13] E. Snelson and Z. Ghahramani, "Variable noise and dimensionality reduction for sparse Gaussian processes," in *Uncertainty in Artificial Intelligence*. AUAI Press, 2006, pp. 461–468.
- [14] P. W. Goldberg, C. K. Williams, and C. M. Bishop, "Regression with input-dependent noise: A Gaussian process treatment," in *NIPS*, 1998, pp. 493–499.
- [15] K. Kersting, C. Plagemann, P. Pfaff, and W. Burgard, "Most likely heteroscedastic Gaussian process regression," in *ICML*, 2007, pp. 393–400.
- [16] N. Quadrianto, K. Kersting, M. D. Reid, T. S. Caetano, and W. L. Buntine, "Kernel conditional quantile estimation via reduction revisited," in *ICDM'09*, 2009, pp. 938–943.
- [17] M. Heinonen, H. Mannerström, J. Rousu, S. Kaski, and H. Lähdesmäki, "Non-stationary Gaussian process regression with hamiltonian monte carlo," in *AISTATS*, 2016, pp. 732–740.
- [18] M. K. Titsias and M. Lázaro-Gredilla, "Variational heteroscedastic Gaussian process regression," in *ICML*, 2011, pp. 841–848.
- [19] M. Menicatas and M. P. Wand, "Variational inference for heteroscedastic semiparametric regression," *Australian & New Zealand Journal of Statistics*, vol. 57, no. 1, pp. 119–138, 2015.
- [20] L. Muñoz-González, M. Lázaro-Gredilla, and A. R. Figueiras-Vidal, "Heteroscedastic Gaussian process regression using expectation propagation," in *MLSP*, 2011, pp. 1–6.
- [21] V. Tolvanen, P. Jylänki, and A. Vehtari, "Expectation propagation for nonstationary heteroscedastic Gaussian process regression," in *MLSP*, 2014, pp. 1–6.
- [22] M. Hartmann and J. Vanhatalo, "Laplace approximation and the natural gradient for Gaussian process regression with the heteroscedastic student-t model," *arXiv preprint arXiv:1712.07437*, 2017.
- [23] L. Muñoz-González, M. Lázaro-Gredilla, and A. R. Figueiras-Vidal, "Divisive Gaussian processes for nonstationary regression," *IEEE Transactions on Neural Networks and Learning Systems*, vol. 25, no. 11, pp. 1991–2003, 2014.
- [24] L. Muñoz-González, M. Lázaro-Gredilla, and A. R. Figueiras-Vidal, "Laplace approximation for divisive Gaussian processes for nonstationary regression," *IEEE Transactions on Pattern Analysis and Machine Intelligence*, vol. 38, no. 3, pp. 618–624, 2016.

- [25] H. Liu, J. Cai, Y.-S. Ong, and Y. Wang, "Understanding and comparing scalable Gaussian process regression for big data," *Knowledge-Based Systems*, vol. 164, pp. 324–335, 2019.
- [26] J. Quiñero-Candela and C. E. Rasmussen, "A unifying view of sparse approximate Gaussian process regression," *Journal of Machine Learning Research*, vol. 6, no. Dec, pp. 1939–1959, 2005.
- [27] M. Titsias, "Variational learning of inducing variables in sparse Gaussian processes," in *AISTATS*, 2009, pp. 567–574.
- [28] Y. Gal, M. van der Wilk, and C. E. Rasmussen, "Distributed variational inference in sparse Gaussian process regression and latent variable models," in *NIPS*, 2014, pp. 3257–3265.
- [29] T. N. Hoang, Q. M. Hoang, and B. K. H. Low, "A distributed variational inference framework for unifying parallel sparse Gaussian process regression models," in *International Conference on Machine Learning*, 2016, pp. 382–391.
- [30] J. Hensman, N. Fusi, and N. D. Lawrence, "Gaussian processes for big data," in *UAI*, 2013, pp. 282–290.
- [31] T. N. Hoang, Q. M. Hoang, and B. K. H. Low, "A unifying framework of anytime sparse Gaussian process regression models with stochastic variational inference for big data," in *ICML*, 2015, pp. 569–578.
- [32] H. Peng, S. Zhe, X. Zhang, and Y. Qi, "Asynchronous distributed variational Gaussian process for regression," in *ICML*, 2017, pp. 2788–2797.
- [33] A. Wilson and H. Nickisch, "Kernel interpolation for scalable structured Gaussian processes (KISS-GP)," in *ICML*, 2015, pp. 1775–1784.
- [34] T. D. Bui and R. E. Turner, "Tree-structured Gaussian process approximations," in *NIPS*, 2014, pp. 2213–2221.
- [35] D. Moore and S. J. Russell, "Gaussian process random fields," in *NIPS*, 2015, pp. 3357–3365.
- [36] G. E. Hinton, "Training products of experts by minimizing contrastive divergence," *Neural Computation*, vol. 14, no. 8, pp. 1771–1800, 2002.
- [37] V. Tresp, "A Bayesian committee machine," *Neural Computation*, vol. 12, no. 11, pp. 2719–2741, 2000.
- [38] M. P. Deisenroth and J. W. Ng, "Distributed Gaussian processes," in *ICML*, 2015, pp. 1481–1490.
- [39] H. Liu, J. Cai, Y. Wang, and Y.-S. Ong, "Generalized robust Bayesian committee machine for large-scale Gaussian process regression," in *International Conference on Machine Learning*, 2018, pp. 3137–3146.
- [40] C. E. Rasmussen and Z. Ghahramani, "Infinite mixtures of Gaussian process experts," in *NIPS*, 2002, pp. 881–888.
- [41] T. Nguyen and E. Bonilla, "Fast allocation of Gaussian process experts," in *ICML*, 2014, pp. 145–153.
- [42] E. Snelson and Z. Ghahramani, "Local and global sparse Gaussian process approximations," in *Artificial Intelligence and Statistics*, 2007, pp. 524–531.
- [43] J. Vanhatalo and A. Vehtari, "Modelling local and global phenomena with sparse Gaussian processes," in *Uncertainty in Artificial Intelligence*. AUAI Press, 2008, pp. 571–578.
- [44] R. Ouyang and K. H. Low, "Gaussian process decentralized data fusion meets transfer learning in large-scale distributed cooperative perception," in *AAAI Conference on Artificial Intelligence*, 2018.
- [45] K. Chalupka, C. K. Williams, and I. Murray, "A framework for evaluating approximation methods for Gaussian process regression," *Journal of Machine Learning Research*, vol. 14, no. Feb, pp. 333–350, 2013.
- [46] M. E. Tipping, "Sparse Bayesian learning and the relevance vector machine," *Journal of Machine Learning Research*, vol. 1, no. Jun, pp. 211–244, 2001.
- [47] C. E. Rasmussen and J. Quiñero-Candela, "Healing the relevance vector machine through augmentation," in *ICML*, 2005, pp. 689–696.
- [48] E. Snelson and Z. Ghahramani, "Sparse Gaussian processes using pseudo-inputs," in *NIPS*, 2006, pp. 1257–1264.
- [49] M. Bauer, M. van der Wilk, and C. E. Rasmussen, "Understanding probabilistic sparse Gaussian process approximations," in *NIPS*, 2016, pp. 1533–1541.
- [50] H. Yu, T. N. Hoang, K. H. Low, and P. Jaillet, "Stochastic variational inference for fully bayesian sparse Gaussian process regression models," *arXiv preprint arXiv:1711.00221*, 2017.
- [51] D. G. Matthews, G. Alexander, M. Van Der Wilk, T. Nickson, K. Fujii, A. Boukouvalas, P. León-Villagrà, Z. Ghahramani, and J. Hensman, "GPflow: A Gaussian process library using TensorFlow," *The Journal of Machine Learning Research*, vol. 18, no. 1, pp. 1299–1304, 2017.
- [52] M. Abadi, P. Barham, J. Chen, Z. Chen, A. Davis, J. Dean, M. Devin, S. Ghemawat, G. Irving, M. Isard *et al.*, "Tensorflow: A system for large-scale machine learning," in *12th {USENIX} Symposium on Operating Systems Design and Implementation*, 2016, pp. 265–283.
- [53] C. E. Rasmussen and H. Nickisch, "Gaussian processes for machine learning (GPML) toolbox," *Journal of Machine Learning Research*, vol. 11, no. Nov, pp. 3011–3015, 2010.
- [54] S. Sun, "A review of deterministic approximate inference techniques for Bayesian machine learning," *Neural Computing and Applications*, vol. 23, no. 7-8, pp. 2039–2050, 2013.
- [55] J. Hensman and N. D. Lawrence, "Nested variational compression in deep Gaussian processes," *arXiv preprint arXiv:1412.1370*, 2014.
- [56] D. P. Kingma and J. Ba, "Adam: A method for stochastic optimization," *arXiv preprint arXiv:1412.6980*, 2014.
- [57] B. Ingram and D. Cornford, "Parallel geostatistics for sparse and dense datasets," in *geoENV VII—Geostatistics for Environmental Applications*. Springer, 2010, pp. 371–381.
- [58] H. Salimbeni, S. Eleftheriadis, and J. Hensman, "Natural gradients in practice: Non-conjugate variational inference in Gaussian process models," in *International Conference on Artificial Intelligence and Statistics*, 2018, pp. 689–697.
- [59] J. Hensman, N. Durrande, and A. Solin, "Variational fourier features for Gaussian processes," *arXiv preprint arXiv:1611.06740*, 2016.
- [60] D. Dheeru and E. Karra Taniskidou, "UCI machine learning repository," 2017. [Online]. Available: <http://archive.ics.uci.edu/ml>
- [61] M. Kaul, B. Yang, and C. S. Jensen, "Building accurate 3D spatial networks to enable next generation intelligent transportation systems," in *MDM*, vol. 1, 2013, pp. 137–146.